Received: 18 July 2023 | Revised: 6 November 2023 | Accepted: 29 December 2023

DOI: 10.1111/ffe.14239

ORIGINAL ARTICLE

FFEMS Fatigue & Fracture of Engineering Materials & Structures WILEY

SIF formula based on exact SIF distribution for semi-elliptical surface cracks subjected to mode I, II, III uniform loading

Yasushi Takase | **Nao-Aki Noda**

Kyushu Institute of Technology, Fukuoka, Japan

Correspondence
Nao-Aki Noda, Kyushu Institute of Technology, 1-1 Sensui-cho Tobata-ku, Kitakyushu-city, Fukuoka 804-8550, Japan.
Email: nao592noda@gmail.com

Abstract

The stress intensity factor (SIF) distribution of a semi-elliptical surface crack is often used for evaluating the fatigue strength of structures. Virtually exact distributions of SIFs F_{ISE},F_{IISE},F_{IIISE} can be provided along the crack front by solving the hypersingular integral equation of the body force method. In this paper, to create a very accurate SIF variation formula, the elliptical crack SIF solutions F_{IE}, F_{IIE}, F_{IIIE} are used and the SIF ratios $F_{\mathrm{ISE}}/F_{\mathrm{IE}}$, $F_{\mathrm{IISE}}/F_{\mathrm{IIE}}$, $F_{\mathrm{IIISE}}/F_{\mathrm{IIIE}}$ are mainly focused. Paying attention to the corner point singularity, by applying the least squares method to the ratio $F_{\mathrm{ISE}}/F_{\mathrm{IE}}$, $F_{\mathrm{IISE}}/F_{\mathrm{IIE}}$ in the whole range of parametric angle β, F_{ISE} and F_{IISE} formulas can be proposed. Instead, F_{IIISE} formula can be proposed by applying the method of least squares to the ratio of $F_{\mathrm{IIISE}}/F_{\mathrm{IIIE}}$ in the range $\beta \geq 15^\circ$ but applying directly to F_{IIISE} in the range $\beta \leq 15^\circ$. In this way, all of formulas proposed in this paper provide the SIFs with better than 1.0% accuracy.

KEYWORDS

calculation formula, crack propagation, distribution of SIF, elliptical crack, semi-elliptical crack, stress intensity factor, surface crack

Highlights

- Accurate SIF formulas for semi-elliptical surface cracks were created within 1% error.
- Similar to solving the HIEM, closed form solutions of an elliptical crack were utilized.
- This formula assume the crack front intersects the free surface at an angle θS≅100.5°.
- Using singularity r-0.5 along the crack front, the shape FISE(β)≈const. was investigated.

1 | INTRODUCTION

Semi-elliptical crack modeling is the most common representation of surface defects. In pressure vessels and general structures, fatigue surface cracks initiate under alternate loading, propagating in a semi-elliptical shape, and eventually cause final failure. The stress intensity factor (SIF) distribution of a semi-elliptical surface crack has been commonly used for predicting the initiation and propagation of brittle and fatigue fractures.[1–8] In the previous studies,[5,9] the problems of a semi-elliptic surface crack in Figure 1A,C were formulated as a system of hypersingular integral equations whose unknown functions are equivalent to crack opening displacements (CODs); then, by solving the equations, the dimensionless SIFs F_{ISE},F_{IISE},F_{IIISE} were provided precisely. By using those solutions, recently, Goto et al. investigated the formation mechanism of inclined fatigue cracks in ultrafine-grained Cu by using the SIF distribution of semi-elliptical surface cracks.[6–8] When using those solutions for experiments and machine design, providing the SIF in a convenient calculation formula is desirable. In this sense, after analyzing notched test specimens, our previous studies provided accurate stress concentration formulas for the whole notch dimensions, which have been widely used conveniently.[10–12]

This paper deals with the dimensionless SIF F_{ISE} formula under remote tension in Figure 1A and also the dimensionless SIFs F_{IISE} and F_{IIISE} formulas under remote shear in Figure 1C. Exact SIF formulas for F_{ISE},F_{IISE},F_{IIISE} will be proposed for semi-elliptic cracks useful for the whole aspect ratio in the range $a/b = 1 \sim 4$. In particular, the exact SIF solution of an elliptical crack in an infinite body F_{IE}, F_{IIE}, F_{IIIE} with $a/b = 1 \sim 4$[13] in Figure 1B,D will be considered since those values are close to F_{ISE}, F_{IISE}, F_{IIISE}. Since the variations of the SIF ratios $F_{\mathrm{ISE}}/F_{\mathrm{IE}}$, $F_{\mathrm{IISE}}/F_{\mathrm{IIE}}$, $F_{\mathrm{IIISE}}/F_{\mathrm{IIIE}}$ are in a small range, it is possible to create highly accurate and practically exact calculation formulas.[12]

In this study, first, the SIF formula to calculate the dimensionless SIF F_{ISE} in Figure 1A will be obtained as a function of the crack aspect ratio to b/a and the

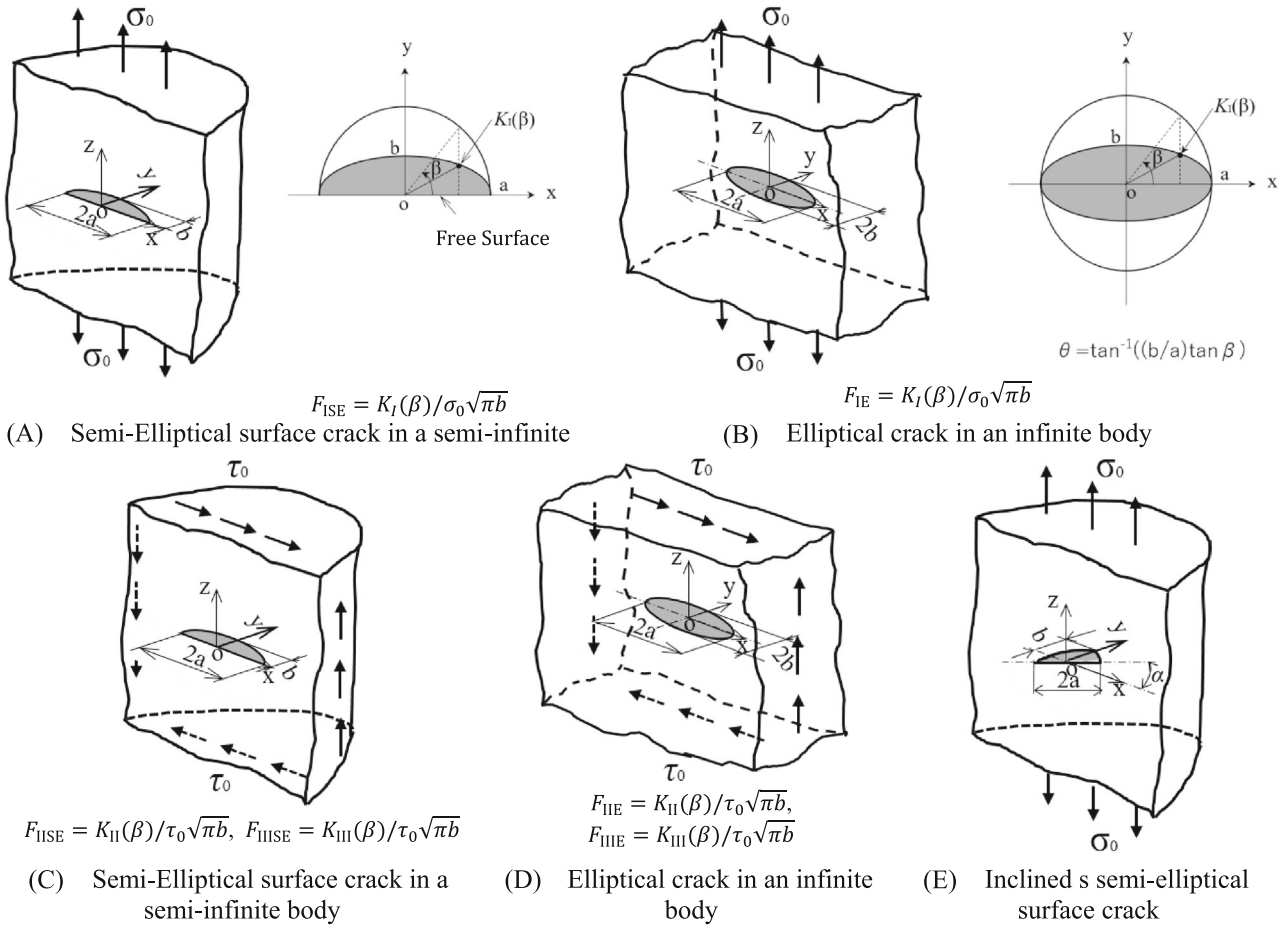

$F_{\mathrm{ISE}} = K_I(\beta)/\sigma_0\sqrt{\pi b}$

(A) Semi-Elliptical surface crack in a semi-infinite

$F_{\mathrm{IE}} = K_I(\beta)/\sigma_0\sqrt{\pi b}$

(B) Elliptical crack in an infinite body

$F_{\mathrm{IISE}} = K_{\mathrm{II}}(\beta)/\tau_0\sqrt{\pi b}$, $F_{\mathrm{IIISE}} = K_{\mathrm{III}}(\beta)/\tau_0\sqrt{\pi b}$

(C) Semi-Elliptical surface crack in a semi-infinite body

$F_{\mathrm{IIE}} = K_{\mathrm{II}}(\beta)/\tau_0\sqrt{\pi b}$,
$F_{\mathrm{IIIE}} = K_{\mathrm{III}}(\beta)/\tau_0\sqrt{\pi b}$

(D) Elliptical crack in an infinite body

(E) Inclined s semi-elliptical surface crack

FIGURE 1 Semi-elliptical surface crack and elliptical crack. (A) Semi-elliptical surface crack in a semi-infinite. (B) Elliptical crack in an infinite body. (C) Semi-elliptical surface crack in a semi-infinite body. (D) Elliptical crack in an infinite body. (E) Inclined semi-elliptical surface crack.

parametric angle β in Figure 1A indicating the position from the free surface. Next, by using the formula obtained, the variation of $F_{\mathrm{ISE}}(\beta)$ will be examined by varying the aspect ratio a/b to investigate the crack shape where $F_{\mathrm{ISE}}(\beta) \approx const$. This is because if the SIF is larger at a certain portion of the surface crack, the portion extends so as to provide a constant SIF along the crack front. Therefore, the shape providing a constant SIF is important since the surface crack becomes larger by maintaining such shape. Moreover, considering mixed mode loading under shear, mode II and mode III SIF formulas will be also provided for the inclined semi-elliptical crack in Figure 1C, where α denotes the inclined angle from the tensile direction.[14] This is because detailed experimental studies require precise distributions of mixed-mode SIFs, which are not provided in a convenient form for machine design. Therefore, similarly to F_{ISE}, highly accurate $F_{\mathrm{IISE}}, F_{\mathrm{IIISE}}$ formulas also will be created.

In creating such a formula, the difference of the SIF between the semi-elliptical crack and elliptical crack will be considered around the corner point $\beta \to 0$. The stress singularity of the semi-elliptic crack is different from the normal crack singularity $r^{-0.5}$ at the corner point where the crack front intersects the free surface (see Appendix A).[14–24] Considering such behavior, accurate calculation formulas will be proposed for the semi-elliptical surface cracks subjected to mode I, II, III uniform loading within 1% error in the range of $1^\circ \le \beta \le 90^\circ$.

2 | STRESS INTENSITY FACTOR DISTRIBUTION ALONG CRACK FRONT OBTAINED BY SOLVING HYPERSINGULAR INTEGRAL EQUATION

In our previous studies, several surface crack problems were formulated as a system of hypersingular integral equations based on the idea of the body force method.[3–5,25,26] The unknown function was then expressed as the product of the fundamental density and polynomial. This method may provide the most accurate solutions to the best of the authors' knowledge (see Appendix B). For the readers' convenience, this section provides the outline of this method. The detail can be seen in references.[3–5,25,26] Consider a semi-infinite body having a semi-elliptical crack as shown in Figure 1A. The problem is reduced to determining the density of force doublet $f(\xi,\eta)$, which is equivalent to COD along the prospective boundary of the crack in the semi-infinite body without a crack. Here, (ξ,η,ς) is a (x,y,z) coordinate where body force doublet is applied[3]

$$\frac{H}{2\pi}\left[\oint\!\!\oint_s \frac{f(\xi,\eta)}{r_1^3}d\xi d\eta + \iint_s K(\xi,\eta,x,y)f(\xi,\eta)d\xi d\eta\right] = -\sigma_z^{\infty}, \tag{1}$$

where

$$\mathrm{K}(\xi,\eta,\mathrm{x},\mathrm{y}) = -\frac{5-20\nu+24\nu^2}{\mathrm{r}_2^3} + \frac{12(1-\nu)(1-2\nu)}{\mathrm{r}_2(\mathrm{r}_2+\mathrm{y}+\eta)^2} + \frac{6\{3\mathrm{y}\eta - 2\nu(1-2\nu)(\mathrm{y}+\eta)^2\}}{\mathrm{r}_2^5},$$

$$\mathrm{r}_1 = \sqrt{(\mathrm{x}-\xi)^2+(\mathrm{y}-\eta)^2}, \quad \mathrm{r}_2 = \sqrt{(\mathrm{x}-\xi)^2+(\mathrm{y}+\eta)^2},$$

$$\mathrm{H} = (1-2\nu)/4(1-\nu)^2,$$

$$\mathrm{S} = \{(\xi,\eta)/(\xi/\mathrm{a})^2 + (\eta/\mathrm{b})^2 \le 1, \eta \ge 0\}.$$

The COD can be defined by using the body force density $f(x',y')$ as shown in Equation (2).[27]

$$U_z(x',y') = u_z(x',y'+0) - u_z(x',y'-0) = \frac{(1-2\nu)(1+\nu)}{E(1-\nu)}f(x',y'),\ x' = x/a,\ y' = y/b \tag{2}$$

Equation (1) can be regarded as the boundary condition at the imaginary boundary of a crack; that is, σ_z=0. The first term in left-hand side of Equation (1) expresses the singular term, and the notation $\oint\!\!\oint_s$ should be interpreted as a finite part integral.[28] In the second term $K(\xi,\eta,x,y)$ means the function that satisfies the boundary condition at the free surface. Here, the unknown function is approximated by using polynomials and the fundamental density function $w(\xi',\eta')$. It should be noted that $w(\xi',\eta')$ exactly expresses the stress field due to an elliptical crack in an infinite body and leads to the semi-elliptical crack solutions with high accuracy. First, we put

$$f(\xi,\eta) = F(\xi',\eta')w(\xi',\eta'),\ w(\xi',\eta') = \frac{b\sigma_z^{\infty}}{H\Phi}\sqrt{1-\xi'^2-\eta'^2},\ \xi' = \xi/a,\ \eta' = \eta/b, \tag{3}$$

where

$$\Phi = \left\{ \begin{array}{l} E(k), k = \sqrt{1-(b/a)^2}\ (a \ge b) \\ \dfrac{b}{a}E(k'),\ k' = \sqrt{1-(b/a)^2}\ (a < b) \end{array} \right\}.$$

Then, the integral Equation (1) becomes

$$\frac{b}{2\pi\Phi}\left[\oint\!\!\oint_s \frac{F(\xi',\eta')}{r_1^3}\sqrt{1-\xi'^2-\eta'^2}\,d\xi d\eta + \int\!\!\int_s K(\xi,\ \eta,\ x,\ y)F(\xi',\eta')\sqrt{1-\xi'^2-\eta'^2}\,d\xi d\eta\right] = -1 \tag{4}$$

Here, $F(\xi',\eta')$ is now approximated in terms of polynomials as follows.

$$\begin{aligned} F(\xi',\eta') = {} & \alpha_0 + \alpha_1\eta' + \cdots \alpha_{n-1}\eta'^{n-1} + \alpha_n\eta'^{n} \\ & + \alpha_{n+1}\xi'^{2\times1} + \alpha_{n+2}\xi'^{2\times1}\eta' + \cdots + \alpha_{2n}\xi'^{2\times1}\eta'^{n-1} \\ & \vdots \qquad\qquad \vdots \\ & + \alpha_{1-2}\xi'^{2(n-1)} + \alpha_{1-2}\xi'^{2(n-1)}\eta' \\ & + \alpha_1\xi'^{2n} \\ = {} & \sum_{i=0}^{1} a_i G_i(\xi',\eta') \end{aligned} \tag{5}$$

$$l = \sum_{k=0}^{n}(k+1) = \frac{(n+1)(n+2)}{2},$$

$$G_0(\xi',\eta') = 1, G_1(\xi',\eta') = \eta', \cdots, G_{n+1}(\xi',\eta') = \xi'^{2\times1}, \cdots, G_l(\xi',\eta') = \xi'^{2\cdot n}$$

Using the approximation method mentioned above, the following linear equations are obtained for the determination of the coefficients α_i. The unknown coefficients α_i $[i=0,1,2...l,\ l=(1/2)(n+1)(n+2)]$ are then determined from (6) by selecting a set of collocation points.

$$\begin{aligned} & \frac{b}{2\pi\Phi}\sum_{i=0}^{l}\alpha_i(A_i+B_i) = -1,\ i=0,\ 1,\ 2.....l, \\ & l = \left(\frac{1}{2}\right)(n+1)(n+2), \\ & A_i = \oint\!\!\oint_s \frac{G_i(\xi',\eta')}{r_1^3}\sqrt{1-\xi'^2-\eta'^2}\,d\xi d\eta, \\ & B_i = \int\!\!\int_s K(\xi,\ \eta,\ x,\ y)G_i(\xi',\eta')\sqrt{1-\xi'^2-\eta'^2}\,d\xi d\eta. \end{aligned} \tag{6}$$

$$\begin{aligned} & M_I\beta = \frac{K_{ISE}\beta}{K_{IE}\beta} = F\xi'\eta'|_{\xi'=cos\beta,\ \eta'=sin\beta}, \\ & K_{IE}\beta = \frac{\sigma_z^{\infty}\sqrt{\pi b}}{\Phi}\left[sin^2\beta + \frac{b^2}{a}\,cos^2\beta\right]^{1/4}, F_{ISE}\beta \\ & = \frac{K_{ISE}\beta}{\sigma_z^{\infty}\sqrt{\pi b}} = \frac{F\xi'\eta'|_{\xi'=cos\beta,\eta'=sin\beta}}{\Phi}\left[sin^2\beta + \frac{b^2}{a}\,cos^2\beta\right]^{1/4}. \end{aligned} \tag{7}$$

Figure 2 shows the boundary collocation points. At the intersection points of the mesh whose interval is 0.02, the boundary conditions are considered to minimize the stress σ_z at the collocation points by applying the least square method. Numerical calculations have been carried out for changing n in (7).

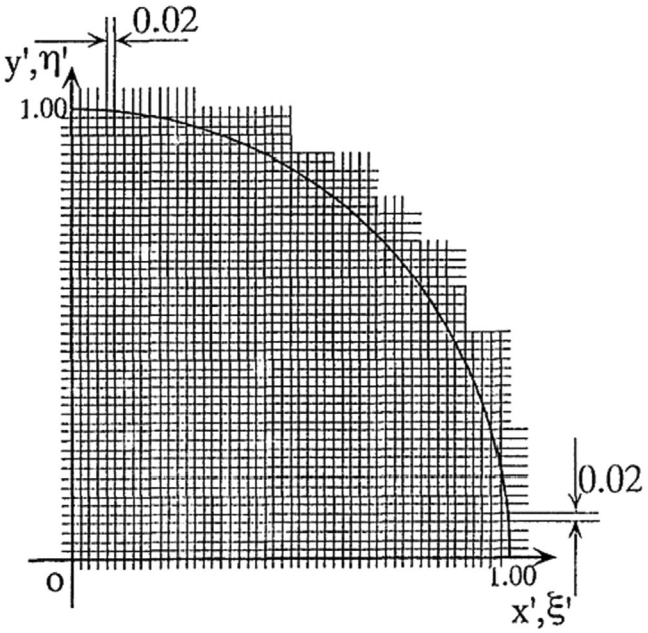

FIGURE 2 Boundary collocation points.

Tables 1 and 2 show the convergency of dimensionless SIFs along the crack front with increasing parameter n in Equation (6). When Poisson's ratio $\nu=0$, Table 1 shows that the results have the convergency to the 5 significant digits for most cases. When $\nu=0$, $a/b=1$, the maximum value of the SIF $F_{ISE}^{Max}=0.7687$ appears at $\beta=0$.

When $\nu=0.3$, Table 2 shows that the results have the convergency in the 4 significant digits for most cases when $n=19$ and in the 3 significant digits for worst cases in the range $\beta=0\sim10°$. When $\nu=0.3$, $a/b=1$ the maximum value of the SIF $F_{ISE}^{Max}=0.748$ appears at $\beta=3°$. Note that when $\nu=0.3$, as $\beta\to0$, the dimensionless SIF $F_{\mathrm{ISE}}\to0$ as explained in Section 3.1.

3 | FORMULA FOR THE STRESS INTENSITY FACTOR FOR SEMI-ELLIPTICAL SURFACE CRACKS UNDER MODE I LOADING

3.1 | Stress singularity at corner point and stress intensity factor around corner point

The semi-elliptical crack perpendicular to the surface in Figure 1 is commonly used to represent a surface defect.

TABLE 1 Convergency of dimensionless stress intensity factor $F_I(\nu = 0, a/b = 1)$.

	β (°)													
n	**0**	**1**	**2**	**3**	**4**	**5**	**6**	**7**	**8**	**9**	**10**	**15**	**20**	**25**
17	0.76838	0.75147	0.73841	0.72806	0.71962	0.71254	0.70643	0.70107	0.69628	0.69198	0.68809	0.67321	0.66323	0.65620
18	0.76865	0.75154	0.73842	0.72807	0.71965	0.71258	0.70646	0.70109	0.69629	0.69198	0.68809	0.67321	0.66323	0.65621
19	0.76874	0.75152	0.73838	0.72806	0.71966	0.71260	0.70650	0.70111	0.59632	0.69200	0.68811	0.67321	0.66324	0.65622
20	0.76882	0.75154	0.73840	0.72807	0.71967	0.71261	0.70650	0.70112	0.69632	0.69200	0.68811	0.67321	0.66324	0.65622
	β (°)													
n	**30**	**35**	**40**	**45**	**50**	**55**	**60**	**65**	**70**	**75**	**80**	**85**	**90**	
17	0.65104	0.64718	0.64424	0.64195	0.64019	0.63881	0.63774	0.63691	0.63627	0.63581	0.63550	0.63531	0.63523	
18	0.65103	0.64718	0.64424	0.64196	0.64019	0.63881	0.63774	0.63691	0.63628	0.63581	0.63549	0.63530	0.63524	
19	0.65103	0.64718	0.64423	0.64196	0.64019	0.63881	0.63774	0.63691	0.63628	0.63581	0.63549	0.63529	0.63522	
20	0.65103	0.64718	0.64423	0.64196	0.64019	0.63881	0.63774	0.63691	0.63628	0.63581	0.63549	0.63529	0.63522	

TABLE 2 Convergency of dimensionless stress intensity factor $F_I(\nu = 0.3, a/b = 1)$.

	β (°)												
n	**1**	**2**	**3**	**4**	**5**	**6**	**7**	**8**	**9**	**10**	**15**	**20**	**25**
17	0.7416	0.7467	0.7480	0.7464	0.7430	0.7386	0.7339	0.7294	0.7254	0.7218	0.70782	0.69692	0.68891
18	0.7413	0.7465	0.7477	0.7459	0.7423	0.7379	0.7334	0.7291	0.7252	0.7217	0.70776	0.69696	0.68892
19	0.7418	0.7459	0.7478	0.7456	0.7419	0.7376	0.7333	0.7292	0.7247	0.7214	0.70761	0.69710	0.68890
20	0.7422	0.7456	0.7476	0.7455	0.7410	0.7367	0.7326	0.7287	0.7243	0.7213	0.70758	0.69712	0.68883
	β (°)												
n	**30**	**35**	**40**	**45**	**50**	**55**	**60**	**65**	**70**	**75**	**80**	**85**	**90**
17	0.68219	0.67711	0.67291	0.66950	0.66676	0.66455	0.66274	0.66123	0.66020	0.65934	0.65871	0.65824	0.65797
18	0.68219	0.67710	0.67291	0.66949	0.66677	0.66455	0.66272	0.66126	0.66016	0.65929	0.65868	0.65827	0.65811
19	0.68216	0.67708	0.67287	0.66950	0.66674	0.66456	0.66270	0.66130	0.66014	0.65928	0.65871	0.65834	0.65847
20	0.68211	0.67708	0.67287	0.66950	0.66674	0.66455	0.66271	0.66128	0.66014	0.65930	0.65873	0.65834	0.65849

Figure 3A illustrates the so-called corner point singular stress, the distance from which is denoted by r. The corner point is defined as the point where the crack front intersects the free surface. In semi-elliptical modeling, the intersection angle $\theta_S = 90°$ defining the singularity exponent. The previous studies showed that at the corner point, the stress singularity is different from $r^{-0.5}$ for ordinary cracks if Poisson's ratio $\nu \neq 0$.[23,29–35] Therefore, as shown in Figure 3, the corner point singular stress for symmetric mode deformation is expressed as $\sigma \propto r^{-p_S}$, $\tau \propto r^{-p_S}$. Instead, the corner point singular stress for skew-symmetric deformation is expressed as $\sigma \propto r^{-p_A}$, $\tau \propto r^{-p_A}$.

In Appendix A, previous studies for corner point singularity exponent p_S, p_A are summarized. Although small difference can be seen among those results, it is known that only $\nu = 0$ of Poisson's ratio provides a consistent stress singularity $r^{-0.5}$ along the crack front. This is the reason why the convergency of the SIF solution for $\nu = 0$ is much better than the one for $\nu = 0.3$ (see Table 2). In other words, solving the problem of $\nu = 0$ is much easier than solving the problem of $\nu \neq 0$. When $\nu = 0.3$, the corner point singularity is smaller as $p_S = 0.452 < 0.5$, and therefore, as $\beta \to 0$, the dimensionless SIF $F_{\mathrm{ISE}}(\beta) \to 0$.[25,34]

Figure 3B illustrates the corner point singularity index p_A under skew-symmetric deformation as well as the corner point singularity index p_S under symmetric deformation. When $\nu = 0.3$, the corner point singularity is smaller as $p_A \approx 0.6 > 0.5$. Therefore, under remote shear in Figure 1C, as $\beta \to 0$, $F_{\mathrm{IISE}}(\beta) \to \infty$ and $F_{\mathrm{IIISE}}(\beta) \to \infty$. The effect of corner point may be localized similarly to F_{ISE}, but since the values of F_{IISE}, F_{IIISE} go to infinity, it may be difficult to make the formula exactly reflect the corner point singularity around $\beta = 0$. Therefore, in this paper, the range of $1° \leq \beta \leq 90°$ and $1 \leq a/b \leq 4$ will be considered to make accurate formulas for F_{ISE}, F_{IISE}, F_{IIISE}.

Although the corner point singularity exponent p_S,p_A was described above, the region affected by the corner point singularity has to be specified. Regarding the semicircular surface crack $a/b = 1$ under tension in Figure 1A, when $\nu = 0.3$ the maximum SIF, $F_{ISE}^{Max} = 0.748$ appears at $\beta = 3°$ (see Table 2). As shown in Table A3 in Appendix A, Murakami-Ishida analyzed the maximum SIF and the position of the square surface crack with side length $2a$.[36] The results showed that when $\nu = 0.3$, the maximum SIF F_I^{Max} appears at $y = 4.69 \times 10^{-2} \times a$, which almost coincides with the position of the maximum SIF of the semicircular crack, that is, $y = sin\,3° = 5.24 \times 10^{-2} \times a$. Also, Murakami explained that the region controlled by the corner point singularity is limited in the small range $y = \sim 10^{-3} \times a$, and, therefore, the discussion on the corner point singularity is practically meaningless.

Since the semicircular and semi-elliptical cracks have zero SIF values at the corner point $\beta = 0$, under stable fatigue crack extension,[36] other crack tips may extend further compared to the corner point $\beta = 0$. Therefore, the intersection angle θ_S with the free surface becomes larger than the original $\theta_S = 90°$. Figure 4 shows the singular exponent p_S for symmetric deformation at the corner point when the crack front intersects to the free surface at the angle θ_S.[36] As indicated in reference,[36] the corner point singularity only affects a limited area.

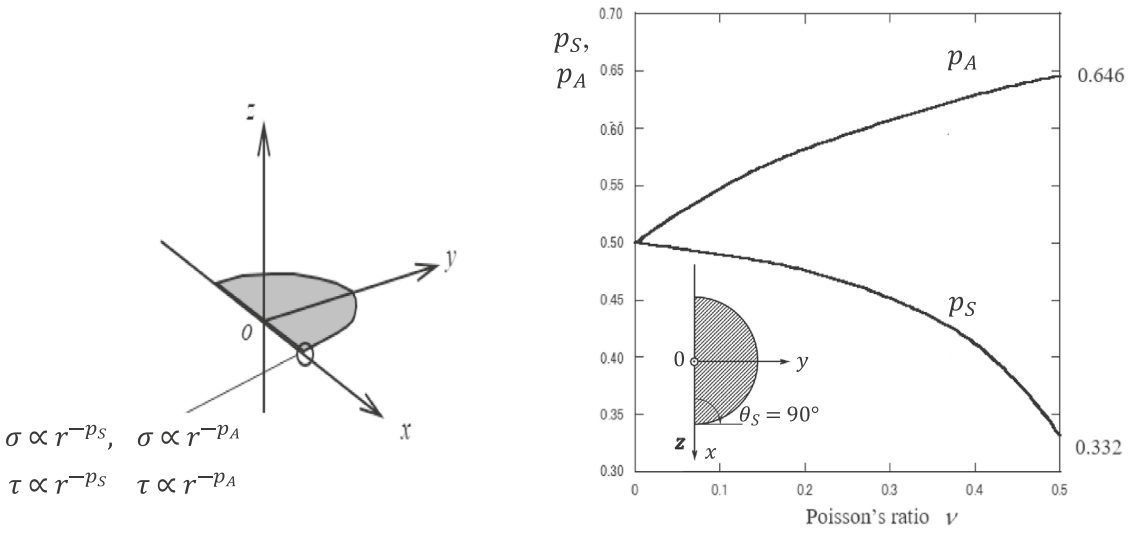

FIGURE 3 Definition of corner point singularity exponents when the crack front intersects to free surface with angle $\theta_S = 90°$. (A) Singular stress at the corner point expressed as $\sigma \propto r^{-p_S}$, $\tau \propto r^{-p_S}$ for symmetric deformation and $\sigma \propto r^{-p_A}$, $\tau \propto r^{-p_A}$ for skew-symmetric deformation. (B) Relation of p_S, p_A versus ν.

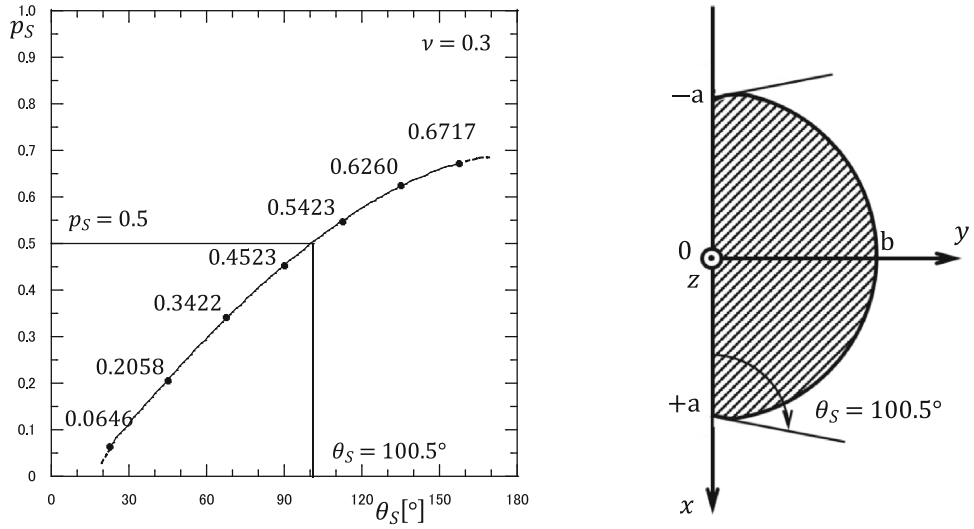

(A) p_S versus θ_S when $\nu = 0.3$ indicating that $p_S = 0.5$ can be provided when $\theta_S \approx 100.5°$.

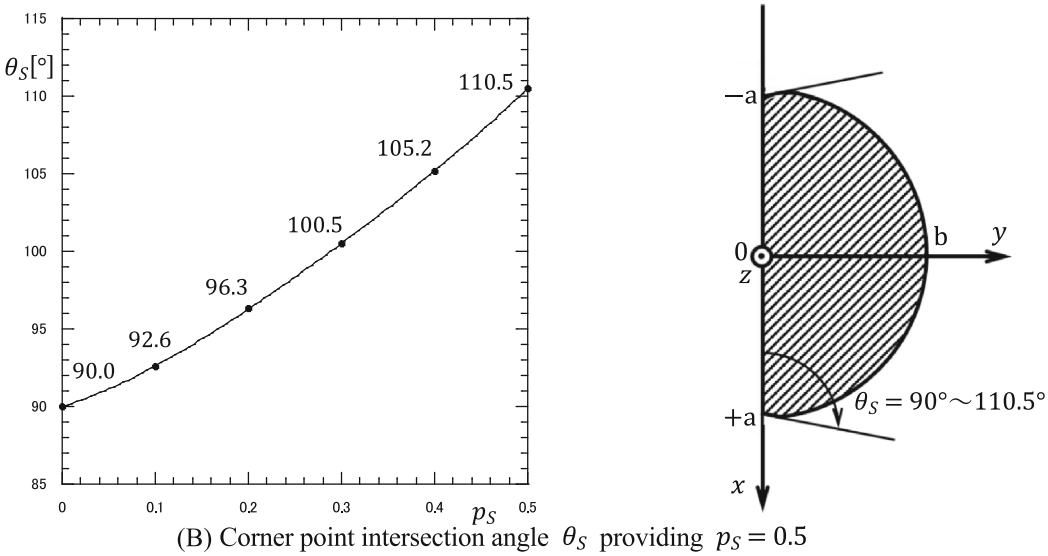

(B) Corner point intersection angle θ_S providing $p_S = 0.5$

FIGURE 4 Corner point singular exponents p_S for symmetric deformation vs crack front angle intersection to free surface θ_S and modified semi-elliptical crack modelling providing $r^{-0.5}$ singularity across the crack front. (A) p_S versus θ_S when $\nu = 0.3$ indicating that $p_S = 0.5$ can be provided when $\theta_S \approx 100.5°$. (B) Corner point intersection angle θ_S providing $p_S = 0.5$.

Therefore, the semi-elliptical modeling should be slightly modified so that the crack front intersects to the free surface at an angle $\theta_S \cong 100.5°$, as shown in Figure 4. This crack model has a stress singularity $r^{-0.5}$ across the crack front including the corner point. In other words, at the corner point, the certain value of SIF should be considered instead of $F_{\mathrm{ISE}}(0) = 0$. In this sense, this paper focuses on $F_{\mathrm{ISE}}(\beta)$ in the range of $\beta = 1° \sim 90°$ without considering $F_{\mathrm{ISE}}(0) = 0$. This paper deals with semi-elliptical cracks in a semi-infinite body under uniform loading as shown in Figure 1. However, since the corner point singularity is meaningless in practice, such semi-elliptical surface crack modeling should be considered such that the crack front intersects the free surface at an angle $\theta_S \cong 100.5°$. This crack model has a stress singularity $r^{-0.5}$ across the crack front including the corner point.

3.2 | Formula for F_{ISE}

Confirming the convergency shown in Tables 1 and 2, when $\nu = 0.3$ and $a/b = 1.0$, 1.33, 2.0, 4.0, the SIFs were obtained[3,26] and indicated in Table 3 as F_{ISE} in the range of $1° \le \beta \le 90°$. Table 3 also shows the SIF values of an elliptical crack F_{IE} in Equation (7).[13] Since the variations of $F_{\mathrm{ISE}}(\beta)$ and $F_{\mathrm{IE}}(\beta)$ are close, the ratio of $F_{\mathrm{ISE}}/F_{\mathrm{IE}}$ is in a narrow range as $1.0344 \sim 1.2875$. Therefore, the least-squares method can be applied to $F_{\mathrm{ISE}}/F_{\mathrm{IE}}$ instead of

TABLE 3 Stress intensity factor F_{ISE}, F_{IE} and ratio of F_{ISE}/F_{IE} ($a/b = 1.0, 1.33, 2.0, 4.0$, $\nu = 0.3$).

	a/b									
	1.0					1.33				
	F_I									
β (°)	F_{ISE} in Ref.[3]	F_{IE} from Equation (7)	$\frac{F_{ISE}}{F_{IE}}$	Equations (8a) and (8b)	Error (%)	F_{ISE} in Ref.[3]	F_{IE} from Equation (7)	$\frac{F_{ISE}}{F_{IE}}$	Equations (8a) and (8b)	Error (%)
1	0.742	0.6366	1.1656	0.7418	−0.03	0.740	0.6269	1.1804	0.7399	−0.02
2	0.746	0.6366	1.1719	0.7467	0.09	0.742	0.6270	1.1834	0.7424	0.06
3	0.748	0.6366	1.1750	0.7476	−0.06	0.743	0.6272	1.1846	0.7426	−0.05
4	0.746	0.6366	1.1719	0.7457	−0.03	0.741	0.6275	1.1809	0.7412	0.02
5	0.742	0.6366	1.1656	0.7423	0.04	0.739	0.6278	1.1771	0.7386	−0.06
6	0.738	0.6366	1.1593	0.7380	−0.01	0.735	0.6282	1.1700	0.7353	0.05
7	0.733	0.6366	1.1514	0.7334	0.05	0.732	0.6287	1.1643	0.7318	−0.03
8	0.729	0.6366	1.1451	0.7289	−0.01	0.728	0.6292	1.1570	0.7282	0.03
9	0.725	0.6366	1.1389	0.7248	−0.03	0.725	0.6298	1.1511	0.7249	−0.01
10	0.721	0.6366	1.1326	0.7212	0.02	0.722	0.6305	1.1451	0.7219	−0.01
20	0.6969	0.6366	1.0947	0.6971	0.03	0.7091	0.6407	1.1068	0.7094	0.04
30	0.6821	0.6366	1.0715	0.6822	0.01	0.7109	0.6554	1.0847	0.7108	−0.01
40	0.6729	0.6366	1.0570	0.6728	−0.01	0.7197	0.6721	1.0708	0.7197	0.00
50	0.6667	0.6366	1.0473	0.6667	0.01	0.7312	0.6887	1.0618	0.7313	0.01
60	0.6627	0.6366	1.0410	0.6627	0.00	0.7424	0.7032	1.0557	0.7424	0.00
70	0.6601	0.6366	1.0369	0.6601	−0.01	0.7515	0.7144	1.0519	0.7515	0.00
80	0.6587	0.6366	1.0347	0.6587	0.00	0.7574	0.7215	1.0498	0.7575	0.01
90	0.6585	0.6366	1.0344	0.6585	0.00	0.7598	0.7239	1.0497	0.7598	0.01

TABLE 3 (Continued)

	a/b									
	2.0					4.0				
	F_I									
β (°)	F_{ISE} in Ref.[3]	F_{IE} from Equation (7)	$\frac{F_{ISE}}{F_{IE}}$	Equations (8a) and (8b)	Error (%)	F_{ISE} in Ref.[3]	F_{IE} from Equation (7)	$\frac{F_{ISE}}{F_{IE}}$	Equations (8a) and (8b)	Error (%)
1	0.710	0.5840	1.2158	0.7096	−0.06	0.601	0.4668	1.2875	0.6009	−0.02
2	0.704	0.5844	1.2047	0.7049	0.13	0.583	0.4684	1.2447	0.5831	0.02
3	0.702	0.5851	1.1999	0.7018	−0.03	0.573	0.4710	1.2166	0.5735	0.08
4	0.700	0.5860	1.1946	0.6996	−0.06	0.570	0.4746	1.2011	0.5696	−0.08
5	0.698	0.5872	1.1888	0.6977	−0.04	0.570	0.4790	1.1899	0.5696	−0.08
6	0.696	0.5886	1.1825	0.6960	0.00	0.572	0.4843	1.1811	0.5721	0.02
7	0.694	0.5903	1.1757	0.6942	0.03	0.576	0.4903	1.1747	0.5763	0.04
8	0.692	0.5922	1.1686	0.6925	0.07	0.581	0.4970	1.1691	0.5813	0.05
9	0.691	0.5943	1.1627	0.6909	−0.02	0.587	0.5042	1.1642	0.5869	−0.02
10	0.690	0.5967	1.1565	0.6896	−0.06	0.593	0.5119	1.1585	0.5928	−0.03
20	0.7044	0.6295	1.1190	0.7045	0.02	0.6767	0.6007	1.1265	0.6769	0.03
30	0.7382	0.6716	1.0992	0.7380	−0.02	0.7661	0.6884	1.1129	0.7660	−0.02
40	0.7767	0.7143	1.0874	0.7767	0.00	0.8446	0.7637	1.1059	0.8447	0.02
50	0.8128	0.7526	1.0800	0.8129	0.02	0.9092	0.8251	1.1020	0.9093	0.01
60	0.8429	0.7840	1.0752	0.8429	0.00	0.9592	0.8723	1.0996	0.9591	−0.01
70	0.8653	0.8070	1.0723	0.8651	−0.02	0.9950	0.9059	1.0984	0.9947	−0.03
80	0.8788	0.8210	1.0704	0.8789	0.01	1.0162	0.9259	1.0975	1.0164	0.02
90	0.8835	0.8257	1.0700	0.8833	−0.03	1.0234	0.9326	1.0974	1.0231	−0.03

directly applied to F_{ISE}, to obtain a highly accurate formula (12). The use of F_{IE} in creating F_{ISE} formula is exactly the same as the use of $w(\xi',\eta')$ in Equation (3) in solving the hypersingular integral Equation (1) for semi-elliptical cracks.

As described in Section 3.1, since the singularity exponent at the corner point $p_S = 0.452 < 0.5$ is weaker compared to the other crack front, $F_{\mathrm{ISE}} \to 0$ as $\beta \to 0$. Corner point effect appears in the range $\beta = 3^\circ \sim \beta = 1^\circ$ as a decrease of F_{ISE}. The effect of the corner point is localized and limited in the range of $\beta \le 3^\circ$. Therefore, in the range of $1^\circ \le \beta \le 90^\circ$ and $1 \le a/b \le 4$ targeted in this paper, the effect of the corner point is more limited, and the ratio $F_{\mathrm{ISE}}/F_{\mathrm{IE}}$ is in the range $F_{\mathrm{ISE}}/F_{\mathrm{IE}} = 1.0344 \sim 1.2875$. Furthermore, the applicable range of the formula is into two parts, that is, $1^\circ \le \beta \le 20^\circ$ and $10^\circ \le \beta \le 90^\circ$; then, the ratio's range $F_{\mathrm{ISE}}/F_{\mathrm{IE}}$ can be smaller. In this way, the following formulas (8a) and (8b) can be created by applying the least squares method to the ratio of $F_{\mathrm{ISE}}/F_{\mathrm{IE}}$ in Table 3. The accuracy of the formulas can be estimated as within 0.2% compared to the F_{ISE} values in Table 3 in the range $1^\circ \le \beta \le 90^\circ$ and $1 \le a/b \le 4$.

When $1^\circ \le \beta \le 20^\circ \pi(/180 \le \beta \le \pi/9)$, $1.0 \le a/b \le 4.0$:

$$
\begin{aligned}
F_{ISE}/F_{IE} &= 1.5713 - 1.1221(b/a) + 1.0408(b/a)^2 - 0.34133(b/a)^3 \\
&+ \left[-0.18718 + 0.56557(b/a) - 0.53103(b/a)^2 + 0.17466(b/a)^3\right]\beta \\
&+ \left[0.032013 - 0.085978(b/a) + 0.063788(b/a)^2 - 0.015795(b/a)^3\right]\beta^2 \\
&+ \left[-0.0026331 + 0.0054534(b/a) - 0.0017899(b/a)^2 - 0.00046795(b/a)^3\right]\beta^3 \\
&+ \left[-0.00010321 - 0.00013791(b/a) - 8.9406\times10^{-5}(b/a)^2 + 0.00010013(b/a)^3\right]\beta^4 \\
&+ \left[-1.5484\times10^{-6} + 8.3237\times10^{-7}(b/a) + 3.9337\times10^{-6}(b/a)^2 - 2.833\times10^{-6}(b/a)^3\right]\beta^5 \\
&\quad (1.0947 \le F_{ISE}/F_{IE} \le 1.2875,\ 0.570 \le F_{ISE} \le 0.748)
\end{aligned}
\tag{8a}
$$

When $10^\circ \le \beta \le 90^\circ (\pi/18 \le \beta \le \pi/2)$, $1.0 \le a/b \le 4.0$:

$$
\begin{aligned}
F_{ISE}/F_{IE} &= 1.1879 + 0.21553(b/a) - 0.3688(b/a)^2 + 0.15787(b/a)^3 \\
&+ \left[-0.00712 - 0.010195(b/a) + 0.018019(b/a)^2 - 0.0081504(b/a)^3\right]\beta \\
&+ \left[0.00029402 - 1.8046\times10^{-5}(b/a) - 0.00025984(b/a)^2 + 0.00014923(b/a)^3\right]\beta^2 \\
&+ \left[-5.6483\times10^{-6} + 4.0129\times10^{-6}(b/a) + 5.2159\times10^{-7}(b/a)^2 - 9.9946\times10^{-7}(b/a)^3\right]\beta^3 \\
&+ \left[5.1738\times10^{-8} - 5.46\times10^{-8}(b/a) + 1.7392\times10^{-8}(b/a)^2 - 6.4006\times10^{-11}(b/a)^3\right]\beta^4 \\
&+ \left[-1.8135\times10^{-10} + 2.2527\times10^{-10}(b/a) - 9.5656\times10^{-11}(b/a)^2 + 1.77\times10^{-11}(b/a)^3\right]\beta^5 \\
&\quad (1.0344 \le F_{ISE}/F_{IE} \le 1.1585, 0.593 \le F_{ISE} \le 1.0234)
\end{aligned}
\tag{8b}
$$

3.3 | Distribution of F_{ISE} provided by formula

Figure 5 illustrates the variations of the ratio F_{ISE}/F_{IE} provided by the created formulas (8a) and (8b). The difference between the elliptical crack and the semi-elliptical crack becomes larger around the corner point due to the different singularity exponent. Figure 6 illustrates the variations of $F_{\mathrm{ISE}}(\beta)$ obtained by multiplying the formulas (8a) and (8b) by the exact solution $F_{\mathrm{IE}}(\beta)$ in Equation (7).

As shown in Figure 6, when $a/b = 1.27 \sim 4.0$, the maximum value of $F_{\mathrm{ISE}}(\beta)$ appears at $\beta = 90°$. Instead,

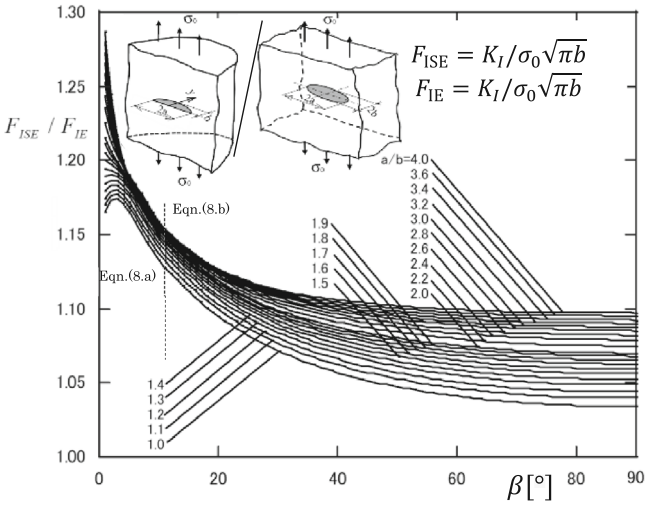

FIGURE 5 $F_{\mathrm{ISE}}/F_{\mathrm{IE}}$ provided by Equations (8a) and (8b).

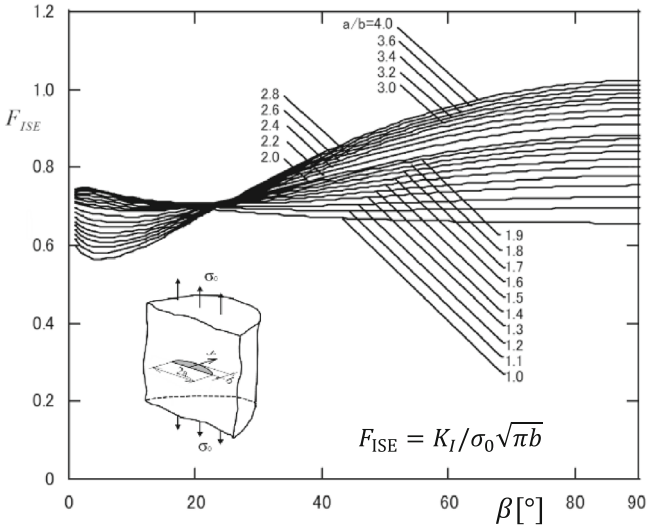

FIGURE 6 F_{ISE} provided by Equation (8).

when $a/b = 1.0 \sim 1.27$, the maximum value of $F_{\mathrm{ISE}}(\beta)$ appears at $\beta = 3°$. When Poisson's ratio $\nu = 0$, as shown in Table 1, the maximum value of $F_{\mathrm{ISE}}(\beta)$ appears at $\beta = 0$. When $\nu = 0.3$, due to the different singularity exponent at the corner point, $F_{\mathrm{ISE}}(\beta) \to 0$ as $\beta \to 0$. This is the reason why the maximum values appear at $\beta = 3°$ when a/b=1.0 ~ 1.27.[25,34]

Consider stable crack growth in metal fatigue. Alternate loading allows the semi-elliptical surface crack with $a/b \approx 1$ to expand in size by increasing a/b, since the point around $\beta \approx 3°$ has the maximum SIF. Instead, the semi-elliptical crack with $a/b \approx 1.5$ has the maximum SIF at the point around $\beta = 90°$, so the size can be enlarged by decreasing a/b. Thus, a semi-elliptical surface crack tends to change shape along the crack front such that $F_{\mathrm{ISE}}(\beta) \approx const$. Therefore, the aspect ratio a/b that satisfies $F_{\mathrm{ISE}}(\beta) \approx const$ should be investigated using Equation (1).

By varying a/b, Figure 7 illustrates the maximum value F_{ISE}^{Max}, the minimum value F_{ISE}^{Min}, the difference $\Delta F = F_{ISE}^{Max} - F_{ISE}^{Min}$, the average value $F_{ISE}^{Ave.}$, and the standard deviation F_{ISE}^{SD}. Since the maximum value appears at $\beta \approx 3°$ or $\beta = 90°$ depending on a/b, both of the local maximum values $F_{ISE}^{Max}\big|_{\beta \cong 3°}$ and $F_{ISE}^{Max}\big|_{\beta = 90°}$ are indicated in Figure 7. As shown in Equation (9), those values are obtained from the data of the created formulas (8a) and (8b) in increments of 1°, that is, the values of $F_{ISE}^{SD}(\beta)$ when $\beta = 1°, 2°, 3°..., 90°$.

$$F_{ISE}^{Ave.} \equiv \frac{1}{N}\sum_{i=1}^{N} F_{ISE}(i(deg.)), \qquad (9)$$

$$F_{ISE}^{SD} \equiv \frac{1}{N}\sqrt{\sum_{i=1}^{N}\left(F_{ISE}(i(deg.)) - F_{ISE}^{Ave.}\right)^2},\ N = 90.$$

Figure 7B shows the details of $F_{ISE}^{Max}\big|_{\beta \cong 3°}$, $F_{ISE}^{Max}\big|_{\beta = 90°}$, $F_{ISE}^{Min}\big|_{\beta = 4° \sim 90°}$, $F_{ISE}^{Ave.}$ when $a/b = 1.0 \sim 1.5$. Figure 7C shows the details of the difference $\Delta F = F_{ISE}^{Max}\big|_{\beta \cong 90°} - F_{ISE}^{Min}\big|_{\beta = 4° \sim 90°}$, $\Delta F = F_{ISE}^{Max}\big|_{\beta \cong 90°} - F_{ISE}^{Min}\big|_{\beta = 4° \sim 90°}$, F_{ISE}^{SD} when $a/b = 1.0 \sim 1.5$. From Figure 7C, the minimum value of the standard deviation occurs at $a/b = 1.20 \sim 1.21$. The difference between the maximum and minimum values $\Delta F = F_{ISE}^{Max}\Big|_{\substack{\beta \cong 3° or \\ \beta = 90°}} - F_{ISE}^{Min}\Big|_{\beta = 4° \sim 90°}$ takes the minimum value at $a/b = 1.27$.

Figure 8 illustrates the maximum values of SIF $F_{ISE}^{Max}\Big|_{\substack{\beta \cong 3° or \\ \beta = 90°}} = K_{ISE}^{Max}/\left(\sigma_0\sqrt{\pi b}\right)$ by varying a/b. As shown in Figure 8, when $a/b \leq 1.27$, the maximum value F_{ISE}^{Max}

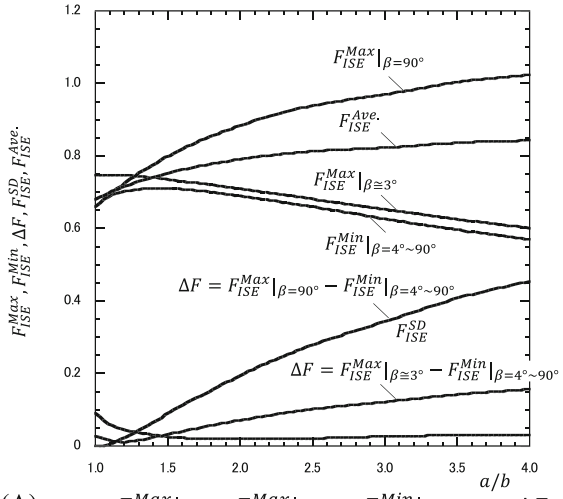

(A) $F_{ISE}^{Max}|_{\beta\approx3°}, F_{ISE}^{Max}|_{\beta=90°}, F_{ISE}^{Min}|_{\beta=4°\sim90°}, \Delta F = F_{ISE}^{Max}|_{\beta=90°} - F_{ISE}^{Min}|_{\beta=4°\sim90°}$, $\Delta F = F_{ISE}^{Max}|_{\beta=90°} - F_{ISE}^{Min}|_{\beta=4°\sim90°}, F_{ISE}^{Ave.}, F_{ISE}^{SD}$ in the range a/b =1.0～4.0

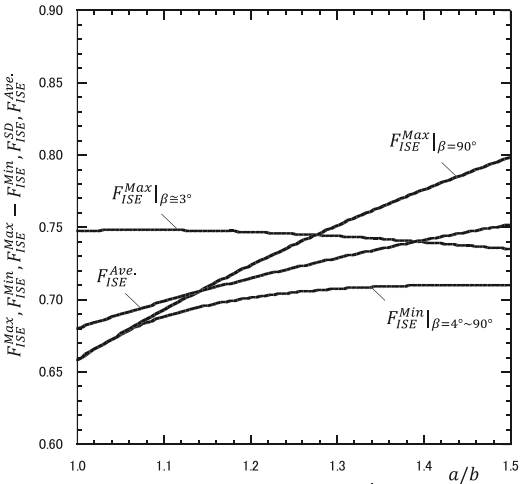

(B) $F_{ISE}^{Max}|_{\beta\cong3°}$, $F_{ISE}^{Max}|_{\beta\cong90°}$, $F_{ISE}^{Min}|_{\beta=4°\sim90°}$, in the range a/b =1.0～1.5

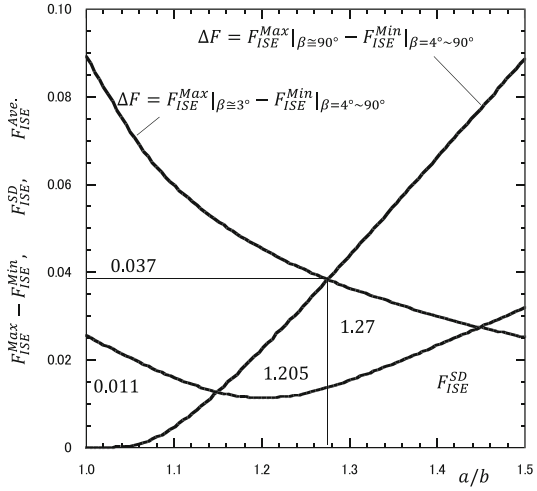

(C) $\Delta F = F_{ISE}^{Max}|_{\substack{\beta\approx3 \text{ or} \\ \beta=90°}} - F_{ISE}^{Min}|_{\beta=4°\sim90°}$ takes the minimum value at a/b =1.27 and F_{ISE}^{SD} takes the minimum value at a/b =1.205

FIGURE 7 Local maximum values $F_{ISE}^{Max}|_{\beta\cong3°}$, $F_{ISE}^{Max}|_{\beta=90°}$, minimum value $F_{ISE}^{Min}|_{\beta=4°\sim90°}$, difference $\Delta F = F_{ISE}^{Max}|_{\beta=90°} - F_{ISE}^{Min}|_{\beta=4°\sim90°}$, difference $\Delta F = F_{ISE}^{Max}|_{\beta\cong3°} - F_{ISE}^{Min}|_{\beta=4°\sim90°}$, average value $F_{ISE}^{Ave.}$, and standard deviation F_{ISE}^{SD} of the SIF of a semi-elliptical crack when $\nu = 0.3$. (A) $F_{ISE}^{Max}|_{\beta\approx3°}$, $F_{ISE}^{Max}|_{\beta=90°}$, $F_{ISE}^{Min}|_{\beta=4°\sim90°}$, $\Delta F = F_{ISE}^{Max}|_{\beta=90°} - F_{ISE}^{Min}|_{\beta=4°\sim90°}$, $\Delta F = F_{ISE}^{Max}|_{\beta=90°} - F_{ISE}^{Min}|_{\beta=4°\sim90°}$, $F_{ISE}^{Ave.}$, F_{ISE}^{SD} in the range a/b =1.0～4.0. (B) $F_{ISE}^{Max}|_{\beta\cong3°}$, $F_{ISE}^{Max}|_{\beta\cong90°}$, $F_{ISE}^{Min}|_{\beta=4°\sim90°}$, in the range $a/b = 1.0 \sim 1.5$. (C) $\Delta F = F_{ISE}^{Max}\Big|_{\substack{\beta\cong3\,or \\ \beta=90°}} - F_{ISE}^{Min}\Big|_{\beta=4°\sim90°}$ takes the minimum value at $a/b = 1.27$ and F_{ISE}^{SD} takes the minimum value at $a/b = 1.205$

appears at $\beta = 3°$, and when $a/b > 1.27$, it appears at $\beta = 90°$. Then, $F_{ISE}^{Max}\Big|_{\substack{\beta\cong3° \text{ or} \\ \beta=90°}}$ takes the smallest value at a/b =1.27. Similarly, as shown in Figure 7, $\Delta F = F_{ISE}^{Max}\Big|_{\substack{\beta\cong3° \text{ or} \\ \beta=90°}} - F_{ISE}^{Min}\Big|_{\beta=4°\sim90°}$ takes the smallest value at a/b=1.27. Since the difference between the maximum and minimum values is smallest, fatigue surface cracks

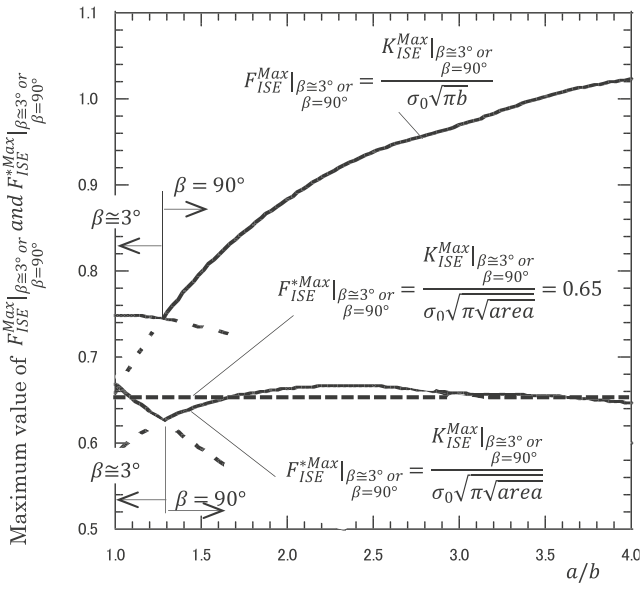

FIGURE 8 Maximum value of the SIF defined as $F_{ISE}^{Max}\Big|_{\substack{\beta\cong3^\circ\ or\\ \beta=90^\circ}} - K_{ISE}^{Max}\Big|_{\substack{\beta\cong3^\circ or\\ \beta=90^\circ}} / \left(\sigma_0\sqrt{\pi b}\right)$ and $F_{ISE}^{*Max}\Big|_{\substack{\beta\cong3^\circ\ or\\ \beta=90^\circ}} - K_{ISE}^{Max}\Big|_{\substack{\beta\cong3^\circ or\\ \beta=90^\circ}} / \left(\sigma_0\sqrt{\pi\sqrt{area}}\right)$ when $\nu = 0.3$.

maintain the shape ratio $a/b \approx 1.27$ and enlarge the overall dimensions.

Figure 8 also shows the result in Equation (10a) in comparison with the maximum SIF expressed in Equation (10b).[37]

$$K_{ISE}^{Max}\Big|_{\substack{\beta\cong3^\circ\ or\\ \beta=90^\circ}} - F_{ISE}^{*Max}\Big|_{\beta\cong3^\circ or\ \beta=90^\circ}\sigma_0\sqrt{\pi\sqrt{area}}$$
$$= (0.62\sim0.67)\sigma_0\sqrt{\pi\sqrt{area}} = (0.65\pm0.03)\sigma_0\sqrt{\pi\sqrt{area}},\ area = \pi ab/2 \tag{10a}$$

It is known that the maximum SIFs of an arbitrarily shaped surface crack can be expressed approximately in terms of $\sqrt{area}$ parameter as shown in Equation (10a).

$$K_{ISE}^{Max}\Big|_{\substack{\beta\cong3^\circ\ or\\ \beta=90^\circ}} \approx 0.65\sigma_0\sqrt{\pi\sqrt{area}},\ area = area\ of\ crack \tag{10b}$$

Therefore, by using Equation (10a), the maximum SIF $K_{ISE}^{Max}\Big|_{\beta\cong3^\circ or\ \beta=90^\circ}$ can be estimated within 5% error.

Figure 9 shows the detailed SIF distribution $F_{\mathrm{ISE}}(\beta)$ when $a/b = 1.18\sim1.30$. Since the crack shape is restricted to semi-ellipse, the SIF distribution cannot be exactly constant. However, when $a/b = 1.20\sim1.30$, the SIF distribution is almost constant as $F_{\mathrm{ISE}}(\beta)\approx const.$ For example, when $a/b = 1.27$, $\Delta F = F_{ISE}^{Max} - F_{ISE}^{Min}$ can be minimized as $\Delta F \approx 0.04$ and when $a/b = 1.205$, the standard variation F_{ISE}^{SD} can be minimized as $F_{ISE}^{SD} \approx 0.01$.

4 | FORMULA FOR THE STRESS INTENSITY FACTOR FOR SEMI-ELLIPTICAL SURFACE CRACKS UNDER MODE II LOADING

4.1 | Hypersingular integral equation under mode II loading

Consider a semi-infinite body subjected to shear stress at infinity $\tau_{zx0}^{\infty} = 1$ as shown in Figure 1C where a semi-elliptical crack is on the xy-plane and a free surface is on the zx-plane. On the idea of the body force method, the problem is formulated as a system of singular integral equations whose unknowns are body force densities $f_{yz}(\xi,\eta), f_{zx}(\xi,\eta)$ distributed in a semi-infinite body without cracks.[5,9] Here, (ξ,η,ζ) is a (x,y,z) coordinate where the body force is applied. Equations (11a) and (11b) enforce boundary conditions at the prospective boundary S for crack; that is, $\tau_{yz} = 0$, $\tau_{zx} = 0$. Equation (1) includes singular terms in the form of $1/r^3$, $1/r^5$ 1 corresponding to the ones of an elliptical crack in an infinite body. The notation $\oint\!\!\!\!\!\!\int_s$ should be interpreted as a finite part integral in the region S. The notation $K_{yz}^{f_{zx}}(\xi,\ x,\ y,\ \psi)$ refers to a function that satisfies the boundary condition for free surface.[5,9]

$$\frac{1}{8\pi(1-\nu)}\left[\oint\!\!\!\!\!\!\int_s\left\{\frac{2(1-2\nu)}{r_1^3}+\frac{6\nu(y-\eta)^2}{r_1^5}\right\}f_{yz}(\xi,\eta)d\xi d\eta\right.$$
$$+\oint\!\!\!\!\!\!\int_s\frac{6\nu(x-\xi)(y-\eta)}{r_1^5}f_{zx}(\xi,\eta)d\xi d\eta$$
$$+\int\!\!\int_s K_{yz}^{f_{yz}}(\xi,\ \eta,\ x,\ y,\psi)f_{yz}(\xi,\eta)d\xi d\eta$$
$$\left.+\int\!\!\int_s K_{yz}^{f_{zx}}(\xi,\ x,\ y,\ \psi)f_{zx}(\xi,\eta)d\xi d\eta\right] = 0 \tag{11a}$$

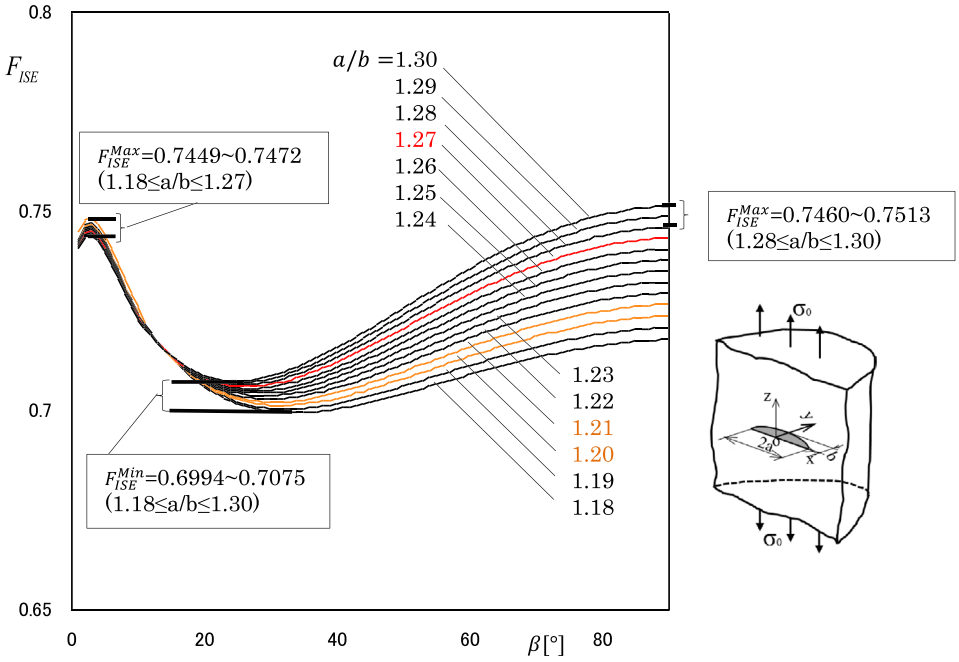

FIGURE 9 Detail of SIF distribution where $F_{\mathrm{ISE}}(\beta)$ is almost constant as $F_{\mathrm{ISE}}(\beta) \approx$ constant at aspect ratio $a/b = 1.18 \sim 1.30$ of semi-elliptical surface cracks. [Colour figure can be viewed at wileyonlinelibrary.com]

$$\frac{1}{8\pi(1-\nu)}\left[\iint_s\left\{\frac{6\nu(x-\xi)(y-\eta)}{r_1^5}\right\}f_{yz}(\xi,\eta)d\xi d\eta + \iint_s\left\{\frac{2(1-2\nu)}{r_1^3}+\frac{6\nu(x-\xi)^2}{r_1^5}\right\}f_{zx}(\xi,\eta)d\xi d\eta + \iint_s K_{zx}^{f_{yz}}(\xi,\eta,x,y,\psi)f_{yz}(\xi,\eta)d\xi d\eta + \iint_s K_{zx}^{f_{zx}}(\xi,x,y,\psi)f_{zx}(\xi,\eta)d\xi d\eta\right] = -1 \tag{11b}$$

$$r_1 = \sqrt{(x-\xi)^2+(y-\eta)^2+(z-\zeta)^2}$$
$$S = \{(\xi,\eta)/(\xi/a)^2+(\eta/b)^2 \le 1,\ \eta \ge 0\} \tag{11c}$$

$$\begin{aligned} U_x(x_a,y_b) &= u_x(x_a,y_b+0)-u_x(x_a,y_b-0) = \frac{2(1-\nu)}{E}f_{zx}(x_a,y_b),\\ U_y(x_a,y_b) &= u_y(x_a,y_b+0)-u_y(x_a,y_b-0) = \frac{2(1-\nu)}{E}f_{yz}(x_a,y_b),\\ U_z(x_a,y_b) &= u_z(x_a,y_b+0)-u_z(x_a,y_b-0) = \frac{(1+2\nu)(1+\nu)}{E(1-\nu)}f_{zz}(x_a,y_b)=0 \end{aligned} \tag{11d}$$

In the numerical solution, the following expressions have been used to approximate the unknown functions $f_{yz}(\xi,\eta))$, $f_{zx}(\xi,\eta)$ as continuous functions.

$$f_{yz}(\xi,\eta) = F_{yz}(\xi_a,\eta_b)w_{yz}(\xi_a,\eta_b),\ f_{zx}(\xi,\eta) = F_{zx}(\xi_a,\eta_b)w_{zx}(\xi_a,\eta_b)$$
$$w_{yz}(\xi_a,\eta_b) = \frac{2b(1-\nu)k^2\tau_{yz0}^{\infty}}{\mathrm{C(k)}}\sqrt{1-\xi_a^2-\eta_b^2},\ \tau_{yz0}^{\infty}=1,$$
$$w_{zx}(\xi_a,\eta_b) = \frac{2b(1-\nu)k^2\tau_{zx0}^{\infty}}{\mathrm{B(k)}}\sqrt{1-\xi_a^2-\eta_b^2},\ \tau_{zx0}^{\infty}=1$$
$$B(k) = (k^2-\nu)E(k)+\nu k'^2K(k),$$
$$C(k) = \left(k^2+\nu k'^2\right)E(k)-\nu k'^2K(k)$$
$$k' = \frac{b}{a}\le 1,\ k = \sqrt{1-\left(\frac{b}{a}\right)^2},\ \xi_a = \frac{\xi}{a\eta_b} = \eta/b$$
$$K(k) = \int_0^{\pi/2}\frac{d\lambda}{\sqrt{1-k^2\sin^2\lambda}}.\ E(k) = \int_0^{\pi/2}\sqrt{1-k^2\sin^2\lambda}d\lambda \tag{12}$$

In Equation (12), $w_{yz}(\xi_a,\eta_b)$, $w_{zx}(\xi_a,\eta_b)$ are called fundamental density functions, which express the exact stress field due to an elliptical crack in an infinite body under the stresses τ_{yz0}^{∞}, τ_{zx0}^{∞} and lead to semi-elliptical crack solutions with high accuracy. In numerical calculations, we can put $\tau_{yz0}^{\infty} = \tau_{zx0}^{\infty} = 1$. Using the expression (12), Equation (11a) is reduced to algebraic equations for the determination of unknown functions $F_{yz}(\xi_a,\eta_b)$, $F_{zx}(\xi_a,\eta_b)$. The SIFs F_{IISE} and F_{IIISE} can be calculated from $F_{yz}(\xi_a,\eta_b)$, $F_{zx}(\xi_a,\eta_b)$ confirming the convergency to the fourth digit. The obtained mode II and mode III SIFs are indicated in Tables 4 and 5.

4.2 | Formula for F_{IISE}

Table 4 summarizes the results for mode II SIF as "F_{IISE} in Ref.[9]", which is obtained from Equations (13) and

TABLE 4 Stress intensity factor F_{IISE}, F_{IIE} and ratio of $F_{\mathrm{IISE}}/F_{\mathrm{IIE}}$ ($a/b = 1.0, 1.33, 1.5, 2.0, 4.0, \nu = 0.3$).

	a/b											
	1.0					1.33					1.5	
	F_{II}											
β (°)	F_{IISE} in Ref.[9]	F_{IIE} from Equation (13)	$\frac{F_{\mathrm{IISE}}}{F_{\mathrm{IIE}}}$	Equations (14a) and (14b)	Error (%)	F_{IISE} in Ref.[9]	F_{IIE} from Equation (13)	$\frac{F_{\mathrm{IISE}}}{F_{\mathrm{IIE}}}$	Equations (14a) and (14b)	Error (%)	F_{IISE} in Ref.[9]	F_{IIE} from Equation (13)
1	0.765	0.749	1.021	1.0203	−0.1027	0.780	0.7660	1.018	1.0166	−0.1605	0.779	0.7660
2	0.744	0.749	0.993	0.9949	0.1634	0.745	0.7660	0.973	0.9762	0.3673	0.740	0.7660
3	0.733	0.748	0.980	0.9796	−0.0385	0.730	0.7650	0.954	0.9543	0.0041	0.723	0.7650
4	0.726	0.747	0.972	0.9710	−0.0893	0.725	0.7640	0.949	0.9452	−0.3950	0.716	0.7630
5	0.720	0.746	0.965	0.9590	−0.6401	0.718	0.7620	0.942	0.9408	−0.1577	0.713	0.7620
6	0.715	0.745	0.960	0.9565	−0.3414	0.714	0.7600	0.939	0.9386	−0.0961	0.709	0.7600
7	0.709	0.743	0.954	0.9542	−0.0069	0.710	0.7580	0.937	0.9365	−0.0171	0.704	0.7570
8	0.704	0.742	0.949	0.9521	0.3504	0.707	0.7560	0.935	0.9346	−0.0629	0.700	0.7550
9	0.700	0.740	0.946	0.9503	0.4561	0.702	0.7530	0.932	0.9328	0.0579	0.695	0.7510
10	0.696	0.738	0.943	0.9486	0.5852	0.697	0.7500	0.929	0.9312	0.1956	0.691	0.7480
20	0.6635	0.7038	0.943	0.9409	−0.1975	0.6479	0.7046	0.920	0.9203	0.0860	0.6342	0.6961
30	0.6139	0.6486	0.947	0.9431	−0.3544	0.5826	0.6348	0.918	0.9166	−0.1225	0.5620	0.6202
40	0.5453	0.5737	0.950	0.9487	−0.1900	0.5021	0.5475	0.917	0.9163	−0.0849	0.4779	0.5291
50	0.4591	0.4814	0.954	0.9532	−0.0551	0.4111	0.4484	0.917	0.9166	−0.0199	0.3871	0.4294
60	0.3580	0.3745	0.956	0.9545	−0.1479	0.3132	0.3416	0.917	0.9162	−0.0745	0.2925	0.3249
70	0.2453	0.2562	0.957	0.9532	−0.4465	0.2108	0.2300	0.917	0.9146	−0.2045	0.1957	0.2177
80	0.1247	0.1301	0.958	0.9518	−0.6950	0.1059	0.1156	0.916	0.9129	−0.3447	0.0980	0.1091
90	0	0	0.960	0.9556	−0.4621	0	0	0.916	0.9131	−0.3159	0	0

TABLE 4 (Continued)

	a/b											
	1.5			2.0				4.0				
	F_{II}											
β (°)	$\frac{F_{IISE}}{F_{IIE}}$	Equations (14a) and (14b)	Error (%)	F_{IISE} in Ref.[9]	F_{IIE} from Equation (13)	$\frac{F_{IISE}}{F_{IIE}}$	Equations (14a) and (14b)	Error (%)	F_{IISE} in Ref.[9]	F_{IIE} from Equation (13)	$\frac{F_{IISE}}{F_{IIE}}$	Equations (14a) and (14b)	Error (%)
1	1.017	1.0159	−0.1090	0.779	0.7500	1.039	1.0382	−0.0459	0.668	0.6360	1.050	1.0499	−0.0439
2	0.966	0.9687	0.2688	0.732	0.7490	0.977	0.9786	0.1283	0.627	0.6340	0.989	0.9892	0.0230
3	0.945	0.9446	−0.0574	0.707	0.7480	0.945	0.9454	0.0183	0.597	0.6300	0.948	0.9483	0.0749
4	0.938	0.9361	−0.2481	0.696	0.7460	0.933	0.9308	−0.2366	0.576	0.6240	0.923	0.9226	−0.0501
5	0.936	0.9348	−0.0927	0.689	0.7430	0.927	0.9272	−0.0124	0.560	0.6170	0.908	0.9031	−0.4960
6	0.933	0.9324	−0.0546	0.684	0.7400	0.924	0.9238	−0.0592	0.547	0.6100	0.897	0.8974	0.0746
7	0.930	0.9301	0.0112	0.679	0.7370	0.921	0.9205	−0.0864	0.535	0.6010	0.890	0.8919	0.1982
8	0.927	0.9279	0.0847	0.673	0.7330	0.918	0.9174	−0.0820	0.524	0.5920	0.885	0.8868	0.1857
9	0.925	0.9259	0.0526	0.666	0.7280	0.915	0.9144	−0.0449	0.513	0.5820	0.881	0.8819	0.0489
10	0.924	0.9240	0.0254	0.659	0.7230	0.911	0.9116	0.0132	0.501	0.5710	0.877	0.8772	−0.0210
20	0.911	0.9110	−0.0082	0.5817	0.6541	0.889	0.8901	0.0865	0.3912	0.4645	0.842	0.8428	0.0686
30	0.906	0.9052	−0.1086	0.4964	0.5650	0.879	0.8776	−0.1145	0.3086	0.3735	0.826	0.8247	−0.1843
40	0.903	0.9027	−0.0598	0.4094	0.4699	0.871	0.8704	−0.1019	0.2434	0.2978	0.817	0.8165	−0.0976
50	0.901	0.9011	−0.0482	0.3241	0.3742	0.866	0.8658	−0.0341	0.1881	0.2313	0.813	0.8135	0.0275
60	0.900	0.8991	−0.1261	0.2410	0.2794	0.863	0.8624	−0.0132	0.1381	0.1702	0.811	0.8125	0.1338
70	0.899	0.8972	−0.1950	0.1597	0.1857	0.860	0.8599	−0.0153	0.0909	0.1121	0.811	0.8124	0.1844
80	0.898	0.8968	−0.1611	0.0798	0.0927	0.861	0.8588	−0.2410	0.0455	0.0557	0.817	0.8137	−0.3947
90	0.903	0.9010	−0.2237	0	0	0.861	0.8610	0.0006	0	0	0.817	0.8186	0.1932

TABLE 5 Stress intensity factor F_{IIISE}, F_{IIIE} and ratio of $F_{\mathrm{IIISE}}/F_{\mathrm{IIIE}}$ ($a/b = 1.0$, 1.33, 1.5, 2.0, 4.0, $\nu = 0.3$).

	a/b											
	1.0					1.33					1.5;	
	F_{III}											
β (°)	F_{IIISE} in Ref.[9]	F_{IIIE} from Equation (15)	$\frac{F_{\mathrm{IIISE}}}{F_{\mathrm{IIIE}}}$	Equations (16a) and (16b)	Error (%)	F_{IIISE} in Ref.[9]	F_{IIIE} from Equation (15)	$\frac{F_{\mathrm{IIISE}}}{F_{\mathrm{IIIE}}}$	Equations (16a) and (16b)	Error (%)	F_{IIISE} in Ref.[9]	F_{IIIE} from Equation (15)
1	0.284	0.009	31.556	0.2832	−0.2725	0.302	0.0120	25.167	0.3014	−0.1933	0.307	0.0140
2	0.238	0.018	13.222	0.2394	0.5864	0.251	0.0250	10.040	0.2520	0.4141	0.257	0.0280
3	0.216	0.027	8.000	0.2166	0.2985	0.227	0.0370	6.135	0.2274	0.1561	0.232	0.0420
4	0.208	0.037	5.622	0.2070	−0.4682	0.219	0.0500	4.380	0.2184	−0.2618	0.223	0.0560
5	0.206	0.046	4.478	0.2047	−0.6534	0.220	0.0620	3.548	0.2185	−0.6613	0.224	0.0700
6	0.206	0.055	3.745	0.2054	−0.2735	0.223	0.0750	2.973	0.2229	−0.0254	0.229	0.0840
7	0.206	0.064	3.219	0.2068	0.3933	0.228	0.0870	2.621	0.2285	0.2290	0.235	0.0980
8	0.206	0.073	2.822	0.2075	0.7150	0.233	0.0990	2.354	0.2336	0.2448	0.242	0.1110
9	0.207	0.082	2.524	0.2071	0.0574	0.237	0.1110	2.135	0.2375	0.2060	0.248	0.1250
10	0.208	0.091	2.286	0.2062	−0.8793	0.242	0.1230	1.967	0.2405	−0.6167	0.254	0.1380
20	0.2509	0.1793	1.399	1.4141	1.0536	0.3129	0.2393	1.308	1.3166	0.6903	0.3381	0.2660
30	0.3108	0.2621	1.186	1.1780	−0.6556	0.3926	0.3420	1.148	1.1433	−0.4047	0.4255	0.3760
40	0.3716	0.3370	1.103	1.1027	0.0009	0.4655	0.4288	1.086	1.0854	−0.0192	0.5022	0.4662
50	0.4273	0.4016	1.064	1.0703	0.5927	0.5266	0.4987	1.056	1.0600	0.3850	0.5648	0.5373
60	0.4739	0.4540	1.044	1.0443	0.0485	0.5743	0.5521	1.040	1.0403	0.0096	0.6127	0.5908
70	0.5088	0.4927	1.033	1.0297	−0.2865	0.6082	0.5897	1.031	1.0286	−0.2727	0.6464	0.6280
80	0.5305	0.5163	1.028	1.0331	0.5483	0.6284	0.6120	1.027	1.0295	0.2620	0.6663	0.6499
90	0.5370	0.5243	1.024	1.0234	−0.0826	0.6348	0.6194	1.025	1.0235	−0.1283	0.6730	0.6571

TABLE 5 (Continued)

	a/b												
	1.5;			2.0				4.0					
	F_{III}												
β (°)	$\frac{F_{IIISE}}{F_{IIIE}}$	Equations (16a) and (16b)	Error (%)	F_{IIISE} in Ref.[9]	F_{IIIE} from Equation (15)	$\frac{F_{IIISE}}{F_{IIIE}}$	Equations (16a) and (16b)	Error (%)	F_{IIISE} in Ref.[9]	F_{IIIE} from Equation (15)	$\frac{F_{IIISE}}{F_{IIIE}}$	Equations (16a) and (16b)	Error (%)
1	21.929	0.3068	−0.0595	0.311	0.0180	17.278	0.3113	0.0971	0.245	0.0310	7.903	0.2454	0.1826
2	9.179	0.2572	0.0882	0.267	0.0370	7.216	0.2662	−0.3142	0.244	0.0620	3.935	0.2431	−0.3878
3	5.524	0.2321	0.0532	0.242	0.0550	4.400	0.2423	0.1237	0.245	0.0920	2.663	0.2448	−0.0886
4	3.982	0.2230	−0.0106	0.233	0.0910	2.560	0.2333	0.1238	0.250	0.1220	2.049	0.2507	0.2782
5	3.200	0.2233	−0.3067	0.234	0.0910	2.571	0.2341	0.0273	0.260	0.1510	1.722	0.2606	0.2172
6	2.726	0.2285	−0.2316	0.241	0.1090	2.211	0.2408	−0.0935	0.274	0.1790	1.531	0.2739	−0.0250
7	2.398	0.2353	0.1436	0.251	0.1090	2.303	0.2506	−0.1466	0.291	0.2070	1.406	0.2902	−0.2874
8	2.180	0.2421	0.0460	0.262	0.1440	1.819	0.2618	−0.0919	0.309	0.2330	1.326	0.3085	−0.1586
9	1.984	0.2480	0.0151	0.273	0.1620	1.685	0.2730	0.0148	0.328	0.2580	1.271	0.3282	0.0489
10	1.841	0.2532	−0.3307	0.284	0.1790	1.587	0.2840	−0.0107	0.348	0.2820	1.234	0.3483	0.0862
20	1.271	1.2782	0.5643	0.3974	0.3333	1.192	1.1974	0.4243	0.5090	0.4734	1.075	1.0775	0.2163
30	1.132	1.1275	−0.3634	0.5003	0.4567	1.095	1.0923	−0.2893	0.6269	0.6039	1.038	1.0367	−0.1339
40	1.077	1.0768	−0.0374	0.5836	0.5520	1.057	1.0568	−0.0400	0.7157	0.6997	1.023	1.0230	0.0098
50	1.051	1.0544	0.3084	0.6484	0.6244	1.038	1.0408	0.2297	0.7836	0.7719	1.015	1.0164	0.1210
60	1.037	1.0371	0.0016	0.6969	0.6776	1.028	1.0284	−0.0123	0.8343	0.8254	1.011	1.0109	0.0155
70	1.029	1.0267	−0.2479	0.7305	0.7143	1.023	1.0211	−0.1569	0.8697	0.8624	1.008	1.0077	−0.0796
80	1.025	1.0274	0.2135	0.7505	0.7358	1.020	1.0216	0.1613	0.8906	0.8843	1.007	1.0077	0.0609
90	1.024	1.0220	−0.2110	0.7566	0.7429	1.018	1.0170	−0.1371	0.8970	0.8915	1.006	1.0056	−0.0559

(14) for $a/b = 1.0$, 1.33, 1.5, 2.0, and 4.0 and $1° \le \beta \le 90°$ when $\nu = 0.3$. The exact solution F_{IISE} of an elliptical crack in an infinite body in Equation (12) is also indicated for comparison.[13] From Table 4, it is seen that the ratio $F_{\mathrm{IISE}}/F_{\mathrm{IIE}}$ is distributed in a narrow range of $F_{\mathrm{IISE}}/F_{\mathrm{IIE}} = 0.811 \sim 1.050$. Since F_{IISE} and F_{IIE} are almost equal widely, the least-squares method can be applied to $F_{\mathrm{IISE}}/F_{\mathrm{IIE}}$ instead of directly applying to obtain a highly accurate formula[12]. The use of F_{IIE} in formulating the formula of F_{IISE} is exactly the same as the use of the solution of an elliptical crack $w_{yz}(\xi_a,\eta_b)$, $w_{zx}(\xi_a,\eta_b)$ in Equation (12) in solving the system of hypersingular integral Equations (11) for semi-elliptical crack.

and the effect of corner point is not so large. In other words, even under the shear loading, the influence of the corner point is localized and limited to just around $\beta = 0$.

To create an accurate formula by reducing the variation range, the whole range for $F_{\mathrm{IISE}}/F_{\mathrm{IIE}}$ is divided into two ranges: one is in the range $1° \le \beta \le 15°$ and the other is in the range $5° \le \beta \le 90°$. Specifically, $F_{\mathrm{IISE}}/F_{\mathrm{IIE}} = 0.908 \sim 1.05$ in the range of $1° \le \beta \le 15°$, and $F_{\mathrm{IISE}}/F_{\mathrm{IIE}} = 0.811 \sim 0.96$ in the range of $15° \le \beta \le 90°$. Then, accurate formulas of $F_{\mathrm{IISE}}/F_{\mathrm{IIE}}$ can be obtained over the entire range of $1° \le \beta \le 90°$.

$$
\begin{aligned}
&For\ \ a > b,\\
&K_{IIE} = \left(\frac{\pi b^3}{a}\right)^{\frac{1}{2}} \times \frac{k^2\tau_0 sin\beta}{\left[\left(k^2-\nu k'^2\right)E(k)+\nu k'^2 K(k)\right]\left(b^2 sin^2\beta + a^2 cos^2\beta\right)^{\frac{1}{4}}},\ k = \left(1-\frac{b^2}{a^2}\right)^{\frac{1}{2}},\ k' = \frac{b}{a}\\
&For\ \ a = \mathrm{b},\ \ K_{IIE} = \frac{4\tau_0\sqrt{a}sin\beta}{(2-\nu)\sqrt{\pi}}\\
&\text{where}\\
&E(k) = \int_0^{\frac{\pi}{2}}\left(1-k^2 sin^2\Phi\right)^{\frac{1}{2}}d\Phi,\ \ K(k) = \int_0^{\frac{\pi}{2}}\frac{d\Phi}{\left(1-k^2 sin^2\Phi\right)^{\frac{1}{2}}},\ F_{\mathrm{IIE}} = K_{\mathrm{IIE}}(\beta)/\tau_0\sqrt{\pi b}
\end{aligned}
\tag{13}
$$

As shown in Table A2 and Figure 3, unlike the SIF under tension, the corner point singularity exponent p_A is larger than that of the normal crack as $p_A = 0.607 > 0.5$. Therefore, F_{IISE} value is supposed to go to infinity as $F_{\mathrm{IISE}} \to \infty$ as $\beta \to 0$. In Table 4, however, in the range of $1° \le \beta \le 90°$ and $1 \le a/b \le 4$, which is the target range in this paper, $F_{\mathrm{IISE}}/F_{\mathrm{IIE}} = 0.811 \sim 1.050$,

The following formulas (14a) and (14b) are created by applying the least squares method to the ratio of $F_{\mathrm{IISE}}/F_{\mathrm{IIE}}$. The values of the formulas are also indicated in Table 4 as Equations (14a) and (14b). As shown in Table 4, the value of F_{IISE} obtained by these formulas has an accuracy within 0.70% of the value of F_{IISE} in Ref.[9] in the range of $a/b = 1.0 \sim 4.0$.

$$
\begin{aligned}
&1° \le \beta \le 5°\,(\pi/180 \le \beta \le \pi/36),\ 1.0 \le a/b \le 4.0:\\
&F_{IISE}/F_{IIE} = 0.75402 + 3.0009(b/a) - 7.6743(b/a)^2 + 7.7609(b/a)^3 - 2.7827(b/a]^4\\
&+\left[-0.11408 + 0.35575(b/a) - 1.8249(b/a)^2 + 2.9235(b/a)^3 - 1.3864(b/a)^4\right]\beta\\
&+\left[0.045929 - 0.32963(b/a) + 1.1559(b/a)^2 - 1.5206(b/a)^3 + 0.65655(b/a)^4\right]\beta^2\\
&+\left[-0.004338 + 0.034715(b/a) - 0.11409(b/a)^2 + 0.14398(b/a)^3 - 0.060793(b/a)^4\right]\beta^3\\
&(0.908 \le F_{IISE}/F_{IIE} \le 1.050,\ 0.560 \le F_{IISE} \le 0.780)
\end{aligned}
\tag{14a}
$$

$$
\begin{aligned}
&5^\circ \le \beta \le 90^\circ (\pi/36 \le \beta \le \pi/2), 1.0 \le a/b \le 4.0:\\
&F_{IISE}/F_{IIE} = 0.82882 + 0.82452(b/a) - 2.0801(b/a)^2 + 2.2124(b/a)^3\\
&-0.81022(b/a)^4\\
&\quad +[-0.014481 + 0.041673(b/a) - 0.069413(b/a)^2 + 0.067052(b/a)^3\\
&\quad -0.028828(b/a)^4)]\beta\\
&\quad +[0.00072004 - 0.004082(b/a) + 0.010009(b/a)^2 - 0.010829(b/a)^3\\
&\quad +0.0043336(b/a)^4)]\beta^2\\
&\quad +[-1.2656\times10^{-5} + 8.5432\times10^{-5}(b/a) - 0.00022474(b/a)^2\\
&\quad +0.0002508(b/a)^3 - 0.00010094(b/a)^4]\beta^3\\
&\quad +[7.5027\times10^{-8} - 5.4711\times10^{-7}(b/a) + 1.4828\times10^{-6}(b/a)^2\\
&\quad -1.6798\times10^{-6}(b/a)^3 + 6.7892\times10^{-7}(b/a)^4]\beta^4\\
&\qquad (0.811 \le F_{IISE}/F_{IIE} \le 0.965,\ 0 \le F_{IISE} \le 0.720)
\end{aligned}
\tag{14b}
$$

Figure 10 illustrates the values of formulas (14a) and (14b) created, and Figure 11 illustrates the values of $F_{\mathrm{IISE}}(\beta)$. From Figure 11, in the range of $1^\circ \le \beta \le 90^\circ$ and $a/b = 1.0 \sim 4.0$, the maximum value of F_{IISE} occurs at $\beta = 0$. Also, around $\beta = 0$, the difference between the and Figure 3, unlike the SIF under tension, the corner point singularity exponent p_A is larger than that of the normal crack as $p_A = 0.607 > 0.5$. Therefore, F_{IIISE} value is supposed to go to infinity as $F_{\mathrm{IIISE}} \to \infty$ as $\beta \to 0$.

$$
\begin{aligned}
&For\ \ a > b,\\
&K_{IIIE} = (\pi ba)^{\frac{1}{2}} \times \frac{-(1-\nu)k^2\tau_0 cos\beta}{\left[(k^2-\nu)E(k) + \nu k'^2 K(k)\right]\left(b^2 sin^2\beta + a^2 cos^2\beta\right)^{\frac{1}{4}}},\ k = \left(1 - \frac{b^2}{a^2}\right)^{\frac{1}{2}},\ k' = \frac{b}{a}\\
&For\ \ a = b,\ \ K_{IIIE} = \frac{4\tau\sqrt{b}(1-\nu)cos\beta}{(2-\nu)\sqrt{\pi}},\\
&\text{where}\\
&E(k) = \int_0^{\frac{\pi}{2}} \left(1 - k^2 sin^2\Phi\right)^{\frac{1}{2}} d\Phi,\ \ K(k) = \int_0^{\frac{\pi}{2}} \frac{d\Phi}{\left(1 - k^2 sin^2\Phi\right)^{\frac{1}{2}}},\ F_{\mathrm{IIIE}} = K_{\mathrm{IIIE}}(\beta)/\tau_0\sqrt{\pi b}
\end{aligned}
\tag{15}
$$

ellipse and the semi-ellipse becomes large due to the influence of the corner point singularity as shown in Figure 9.[25,34]

4.3 | Formula for F_{IIISE}

Table 5 summarizes the results for mode III SIF as "F_{IIISE} in Ref.[9]", which is obtained from Equations (15) and (16) for $a/b = 1.0$, 1.33, 1.5, 2.0, and 4.0 and $1^\circ \le \beta \le 90^\circ$ when $\nu = 0.3$. The exact solution F_{IIIE} of an elliptical crack in an infinite body in Equation (15) is also indicated for comparison.[13] Different from Table 4, Table 5 shows that the ratio $F_{\mathrm{IIISE}}/F_{\mathrm{IIIE}}$ is distributed in a wide range $F_{\mathrm{IIISE}}/F_{\mathrm{IIIE}} = 1.006 \sim 31.6$. As shown in Table A2

Unlike $F_{\mathrm{IISE}}/F_{\mathrm{IIE}}$, in Table 5 at $\beta = 1^\circ \sim 3^\circ$, the value of mode III ratio $F_{\mathrm{IIISE}}/F_{\mathrm{IIIE}}$ is quite large as $F_{\mathrm{IIISE}}/F_{\mathrm{IIIE}} > 10$. However, this is not the effect of corner point, and this is because the denominator of $F_{\mathrm{IIISE}}/F_{\mathrm{IIIE}}$ goes to zero. Because of symmetry, the SIF of the elliptical crack goes to zero as $F_{\mathrm{IIIE}} \to 0$ at $\beta \to 0$. In this way, it is found that when β is small, the ratio $F_{\mathrm{IIISE}}/F_{\mathrm{IIIE}}$ is not suitable to create an accurate formula since $F_{\mathrm{IIIE}} \to 0$ at $\beta \to 0$. Instead, to create an accurate formula, the least squares method should be directly applied to F_{IIISE} when β is small. Specifically, when $1^\circ \le \beta \le 15^\circ$, the direct value of F_{IIISE} is considered considering $F_{\mathrm{IIISE}} = 0.20 \sim 0.42$. When $15^\circ \le \beta \le 90^\circ$, the formula is created for the ratio of $F_{\mathrm{IIISE}}/F_{\mathrm{IIIE}}$ considering $F_{\mathrm{IIISE}}/F_{\mathrm{IIIE}} = 1.01 \sim 1.66$.

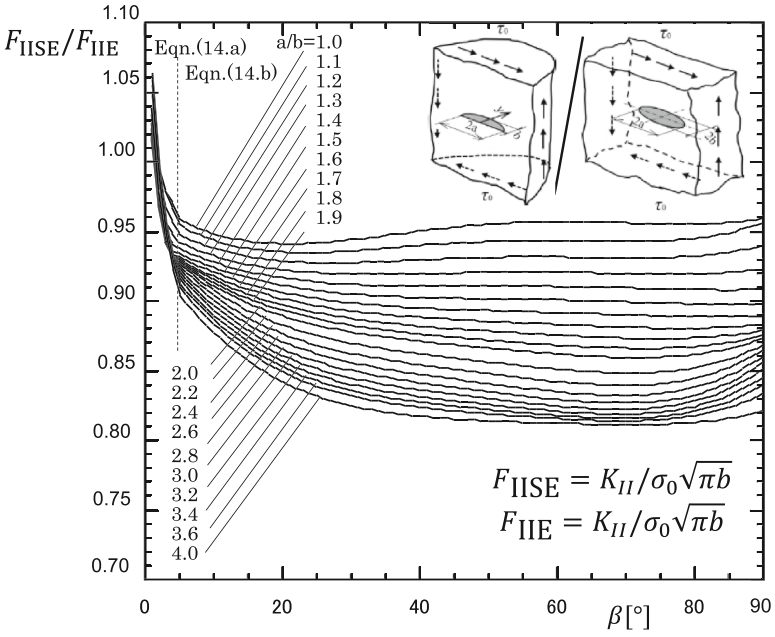

FIGURE 10 $F_{\mathrm{IISE}}/F_{\mathrm{IIE}}$ provided by Equations (14a) and (14b).

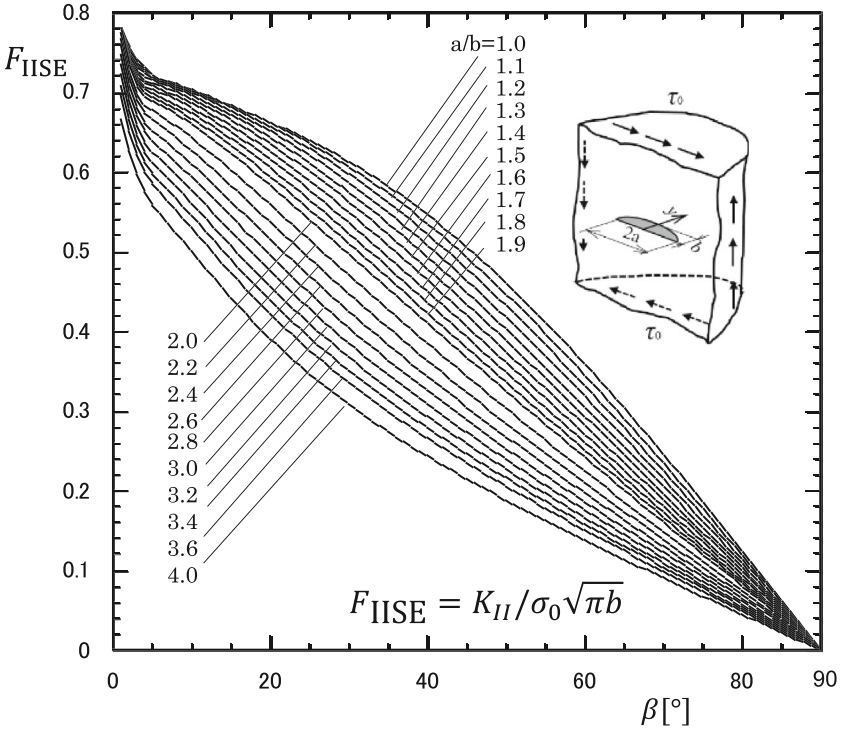

FIGURE 11 F_{IISE} provided by Equation (14).

Formula (16a) is created by applying the least-squares method directly to the values of F_{IISE} in the range of $1° \leq \beta \leq 15°$ shown in Table 5. The calculation formula (16b) created by applying the least squares method to the ratio of $F_{\mathrm{IISE}}/F_{\mathrm{IIE}}$ in the range of $15° \leq \beta \leq 90°$ is shown below. The value of F_{IISE} obtained by these formulas has an accuracy within 1.0% of the value of F_{IISE} of the body force method in the range of $a/b = 1.0 \sim 4.0$.

$$
\begin{aligned}
&1^\circ \le \beta \le 15^\circ (\pi/180 \le \beta \le \pi/12), 1.0 \le a/b \le 4.0:\\
F_{IIISE} = &-0.27209 + 3.3695(b/a) - 6.2961(b/a)^2 + 5.1954(b/a)^3 - 1.6383(b/a)^4\\
&+\left[0.23536 - 1.4621(b/a) + 2.3717(b/a)^2 - 1.7884(b/a)^3 + 0.54852(b/a)^4\right]\beta\\
&+\left[-0.033483 + 0.18208(b/a) - 0.1872(b/a)^2 + 0.076744(b/a)^3 - 0.01615(b/a)^4\right]\beta^2\\
&+\left[0.0023605 - 0.0075409(b/a) - 0.0093679(b/a)^2 + 0.019907(b/a)^3 - 0.0077304(b/a)^4\right]\beta^3\\
&+\left[-7.3948\times10^{-5} - 3.7927\times10^{-5}(b/a) + 0.0014716(b/a)^2 - 0.0019481(b/a)^3 + 0.00070752(b/a)^4\right]\beta^4\\
&+\left[7.9301\times10^{-7} + 5.9261\times10^{-6}(b/a) - 3.9674\times10^{-5}(b/a)^2 + 4.7752\times10^{-5}(b/a)^3 - 1.7016\times10^{-5}(b/a)^4\right]\beta^5\\
&\quad (0.206 \le F_{IIISE} \le 0.4349,\ 1.121 \le F_{IIISE}/F_{IIIE} \le 31.556)
\end{aligned}
\tag{16a}
$$

$$
\begin{aligned}
&15^\circ \le \beta \le 90^\circ \left(\pi/12 \le \beta \le \pi/2, 1.0 \le a/b \le 4.0:\right.\\
&F_{IIISE}/F_{IIIE} = 0.83931 + 2.2047(b/a) + 0.72668(b/a)^2 - 0.2876(b/a)^3\\
&+\left[0.014972 - 0.1954(b/a) - 0.0052608(b/a)^2 - 0.015714(b/a)^3)\right]\beta\\
&+\left[-0.00059058 + 0.0073697(b/a) - 0.0015559(b/a)^2 + 0.0016657(b/a)^3\right]\beta^2\\
&+\left[1.1462\times10^{-5} - 0.00013795(b/a) + 5.3974\times10^{-5}(b/a)^2\right.\\
&\left.-4.5724\times10^{-5}(b/a)^3\right]\beta^3\\
&+\left[-1.0855\times10^{-7} + 1.2625\times10^{-6}(b/a) - 6.7493\times10^{-7}(b/a)^2\right.\\
&\left.+5.2074\times10^{-7}(b/a)^3\right]\beta^4\\
&+\left[3.9866\times10^{-10} - 4.4908\times10^{-9}(b/a) + 2.9252\times10^{-9}(b/a)^2\right.\\
&\left.-2.1409\times10^{-9}(b/a)^3\right]\beta^5\\
&\quad (1.006 \le F_{IIISE}/F_{IIIE} \le 1.668,\ 0.2263 \le F_{IIISE} \le 0.8970)
\end{aligned}
\tag{16b}
$$

Figure 12 illustrates the values of formulas (16a) and (16b) created. Figure 13 illustrates $F_{\mathrm{IIISE}}(\beta)$. From Figure 13, in the range of $1^\circ \le \beta \le 90^\circ$ and $a/b = 1.0 \sim 4.0$, the maximum value of F_{IIISE} occurs at $\beta = 90^\circ$. Also, around $\beta = 0$, $F_{\mathrm{IIISE}} \to \infty$ due to the influence of the corner point singularity, but due to symmetry, $F_{\mathrm{IIISE}} \to 0$, so the difference between ellipse and semi-ellipse becomes very large as shown in Figure 12. In other words, K_{IIISE} finally goes to infinity as can be expressed $K_{\mathrm{IIISE}} \to \infty$ as $\beta \to 0$.

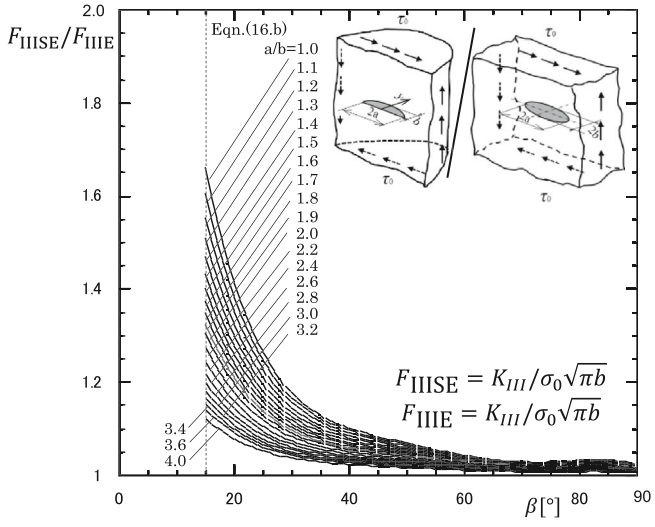

FIGURE 12 $F_{\mathrm{IIISE}}/F_{\mathrm{IIIE}}$ provided by Equation (16b).

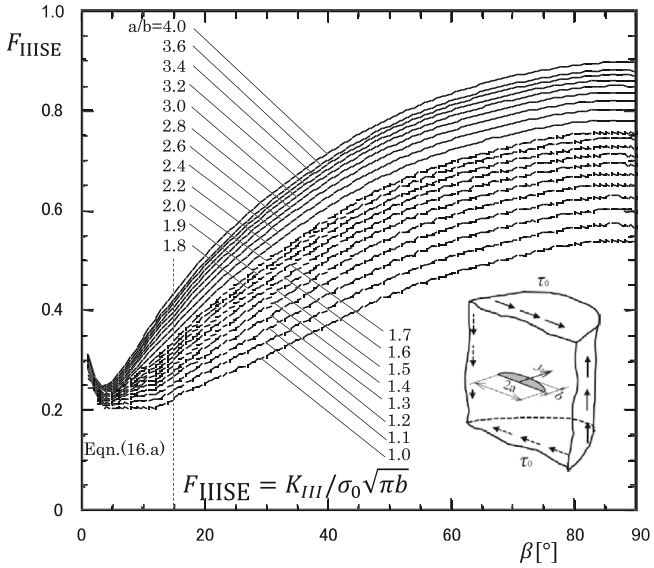

FIGURE 13 F_{IIISE} provided by Equation (16a) and Equation (16b).

Deformation mode	I	II	III
F_{iSE} i = I, II, III	$F_{\mathrm{ISE}} \to 0$ as $\beta \to 0°$	$F_{\mathrm{IISE}} \to \infty$ as $\beta \to 0°$	$F_{\mathrm{IIISE}} \to \infty$ as $\beta \to 0°$
F_{iE} i = I, II, III	$F_{\mathrm{IE}} \to$ Finite as $\beta \to 0°$	$F_{\mathrm{IIE}} \to$ Finite as $\beta \to 0°$	$F_{\mathrm{IIIE}} \to 0$ as $\beta \to 0°$
$\frac{F_{\mathrm{iSE}}}{F_{\mathrm{iE}}}$ i = I, II, III	$F_{\mathrm{ISE}}/F_{\mathrm{IE}} \to 0$ as $\beta \to 0°$	$F_{\mathrm{IISE}}/F_{\mathrm{IIE}} \to \infty$ as $\beta \to 0°$	$F_{\mathrm{IIISE}}/F_{\mathrm{IIIE}} \to \infty$ as $\beta \to 0°$

TABLE 6 Behaver of $F_{\mathrm{ISE}}, F_{\mathrm{IISE}}, F_{\mathrm{IIISE}}$ and $F_{\mathrm{IE}}, F_{\mathrm{IIE}}, F_{\mathrm{IIIE}}$ when $\beta \to 0$.

5 | SUMMARY OF SIF-β RELATION OF SEMI-ELLIPTICAL CRACK IN COMPARISON WITH SIF-β RELATION OF ELLIPTICAL CRACK

Table 6 summarizes the SIF-β relation of a semi-elliptical crack. Regarding mode I SIFs, the relation of the semi-elliptical crack, F_{ISE}-β, is similar to the one of and the elliptical crack, F_{IE}-β, relation except at the corner point. Therefore, the ratio relation, $F_{\mathrm{ISE}}/F_{\mathrm{IE}}$-$\beta$, can be used conveniently to create the calculation formula for almost the whole range. Regarding mode II SIFs, the F_{IIE}-β relation is also similar to the F_{IISE}-β. Therefore, the ratio $F_{\mathrm{IISE}}/F_{\mathrm{IIE}}$-$\beta$ can be used conveniently to create the calculation formula for almost the whole range. It can be concluded that the effect of corner point singularity is localized just around the corner point.

Unlike mode I and mode II, it should be noted that mode III SIF of an elliptical crack goes to zero when β goes to zero. Therefore, F_{IIIE}-β approximation is not suitable

when F_{IIIE} takes relatively smaller value. The calculation formula should be based on the direct value of F_{IIISE}. Considering those behaviors, the accurate SIF formula has been proposed.

6 | CONCLUSIONS

Semi-elliptical crack modeling is the most common representation to express surface defects. Fatigue surface cracks initiate under alternate loading and propagate in a semi-elliptical shape. In this study, based on the exact solutions obtained by the hypersingular integral equation methods, the SIF formulas were created to express the SIF distributions. In particular, similar to solving the hypersingular integral equations by using the solution of an elliptical crack, closed-form SIF distributions of an elliptical crack were utilized. The specific behaviors at the corner point were also considered. The conclusions can be summarized as follows.

1. Under tensile loading in Figure 1A,B, the mode I formula F_{ISE} can be created by focusing on the ratio $F_{\mathrm{ISE}}/F_{\mathrm{IE}}$ in the entire range $1^\circ \le \beta \le 90^\circ$ with less than 1% error. Since the singularity exponent $p_S = 0.452 < 0.5$ at the corner point is weaker than that of normal cracks, $F_{\mathrm{ISE}} \to 0$ when $\beta \to 0$. However, since the effect of the corner point is local and limited to the vicinity of $\beta \cong 0$, it can be confirmed that $F_{\mathrm{ISE}}/F_{\mathrm{IE}}$ is in a narrow range of $F_{\mathrm{ISE}}/F_{\mathrm{IE}} = 1.0344 \sim 1.2875$ for $1^\circ \le \beta \le 90^\circ$.
2. The SIF distribution $F_{\mathrm{ISE}}(\beta)$ obtained by the mode I formula is examined by varying the aspect ratio $a/b = 1.0 \sim 4.0$ under tensile load. It was found that the $\Delta F = F_{ISE}^{Max} - F_{ISE}^{Min}$ takes the smallest value at $a/b = 1.27$. Since the difference between the maximum and minimum values is smallest, fatigue surface cracks maintain the shape ratio $a/b \approx 1.27$ and enlarge the overall dimensions (see Figures 7 and 8).
3. Under shear loading in Figure 1C,D, the mode II formula F_{IISE} can be created by focusing on the ratio $F_{\mathrm{IISE}}/F_{\mathrm{IIE}}$ in the entire range $1^\circ \le \beta \le 90^\circ$ with less than 1% error. Since the singularity exponent $p_A = 0.607 > 0.5$ at the corner point is stronger than that of the normal cracks, $F_{\mathrm{IISE}} \to \infty$ as $\beta \to 0$. However, since the effect of the corner point is local and limited to the vicinity of $\beta \cong 0$, it can be confirmed that $F_{\mathrm{IISE}}/F_{\mathrm{IIE}}$ is in a narrow range of $F_{\mathrm{IISE}}/F_{\mathrm{IIE}} = 0.811 \sim 1.050$ for $1^\circ \le \beta \le 90^\circ$.
4. Under shear loading in Figure 1C,D, the mode III formula F_{IIISE} can be created by focusing on the value of F_{IIISE} directly in the range $1^\circ \le \beta \le 20^\circ$ but focusing on the ratio of $F_{\mathrm{IIISE}}/F_{\mathrm{IIIE}}$ in the range $15^\circ \le \beta \le 90^\circ$ with less than 1% error. Unlike F_{ISE}, F_{IISE}, the direct value of F_{IIISE} should be used because the solution of the elliptical crack is not suitable since $F_{\mathrm{IIIE}} \to 0$ as $\beta \to 0$.

ACKNOWLEDGMENTS

The authors would like to express their sincere gratitude to Dr. Chen Tong at Zhengzhou University for assisting in formulating formulas while conducting this research.

DATA AVAILABILITY STATEMENT

The data that support the findings of this study are available from the corresponding author upon reasonable request.

NOMENCLATURE

a, b	elliptical dimensions in Figure 1
(x,y,z)	Cartesian coordinate in Figure 1
(ξ,η,ζ)	(x,y,z) coordinate where body force is applied
(x',y')	$(x/a, y/b)$
(ξ',η')	$(\xi/a, \eta/b)$
E	Young's modulus
F_{ISE}	dimensionless stress intensity factor for semi-elliptical surface cracks in a semi-infinite body under mode I loading $(F_{\mathrm{ISE}} = K_I(\beta)/\sigma_0\sqrt{\pi b})$
F^*_{ISE}	dimensionless stress intensity factor for semi-elliptical surface cracks normalized by $\sqrt{area}$ $(F^*_{\mathrm{ISE}} = K_I(\beta)/\sigma_0\sqrt{\pi\sqrt{area}})$
F_{IISE}	dimensionless stress intensity factor for semi-elliptic surface cracks in a semi-infinite body under mode II loading $(F_{\mathrm{IISE}} = K_{\mathrm{II}}(\beta)/\tau_0\sqrt{\pi b})$
F_{IIISE}	dimensionless stress intensity factor for semi-elliptical surface cracks in a semi-infinite body under mode III loading $(F_{\mathrm{IIISE}} = K_{\mathrm{III}}(\beta)/\tau_0\sqrt{\pi b})$
F_{IE}	dimensionless stress intensity factor for elliptical cracks in an infinite body under mode I loading $(F_{\mathrm{IE}} = K_I(\beta)/\sigma_0\sqrt{\pi b})$
F_{IIE}	dimensionless stress intensity factor for elliptical cracks in an infinite body under mode II loading $(F_{\mathrm{IIE}} = K_{\mathrm{II}}(\beta)/\tau_0\sqrt{\pi b})$
F_{IIIE}	dimensionless stress intensity factor for elliptical cracks in an infinite body under mode III loading $(F_{\mathrm{IIIE}} = K_{\mathrm{III}}(\beta)/\tau_0\sqrt{\pi b})$
$F^{\mathrm{Max}}_{\mathrm{ISE}}, F^{Min}_{\mathrm{ISE}}$	maximum and minimum dimensionless stress intensity factors for a semi-elliptical surface crack in a semi-infinite field

$F_{\mathrm{ISE}}^{Ave.}$ mean value of dimensionless stress intensity factors for a semi-elliptical surface crack in a semi-infinite body defined in $F_{ISE}^{Ave.} \equiv \frac{1}{N}\sum_{i=1}^{N} F_{ISE}(i(deg.)),\ N = 90$

F_{ISE}^{SD} standard deviation of dimensionless stress intensity factors for a semi-elliptical surface crack in a semi-infinite body defined in $F_{ISE}^{SD} \equiv \frac{1}{N}\sqrt{\sum_{i=1}^{N}\left(F_{ISE}(i(deg.)) - F_{ISE}^{Ave.}\right)^2},\ N = 90$

ΔF difference between maximum and minimum of dimensionless stress intensity factors for a semi-elliptical surface crack ($\Delta F = F_{ISE}^{Max}\big|_{\beta \cong 3^\circ} - F_{ISE}^{Min}\big|_{\beta = 4^\circ \sim 90^\circ}$, $\Delta F = F_{ISE}^{Max}\big|_{\beta = 90^\circ} - F_{ISE}^{Min}\big|_{\beta = 4^\circ \sim 90^\circ}$)

$K_{ISE}^{Max}\big|_{\beta \cong 3^\circ or\ \beta = 90^\circ}$ maximum dimensionless stress intensity factors on the $\beta \cong 3^\circ or \beta = 90^\circ$

$K_{ISE}^{*Max}\big|_{\beta \cong 3^\circ or\ \beta = 90^\circ}$ maximum dimensionless stress intensity factors in $\sqrt{area}$ on the $\beta \cong 3^\circ$

H $(1-2\nu)/4(1-\nu)^2$

M_I dimensionless stress intensity factor

$M_I(x',y')$ dimensionless crack opening displacement

$U_z(x',y')$ crack opening displacement $u_z(x,y,+0)$-$u_z(x,y,-0)$

β parametric angle from free surface (°) specifying ellipse as $(x,y) = (a\cos\beta, b\sin\beta)$

ν Poisson's ratio (in most cases $\nu = 0.3$)

REFERENCES

1. Gopalakrishnan K, Mecholsky JJ. Quantitative fractography of mixed-mode fracture in an R-curve material. *J Mater Sci*. 2013; 48(20):7081-7087.
2. Levesque G, Arakere NK. Empirical stress intensity factors for surface cracks under rolling contact fatigue. *Tribol Trans*. 2010; 53(4):621-629.
3. Noda N-A, Miyoshi S. Variation of stress intensity factor and crack opening displacement of semi-elliptical surface crack. *Int J Fract*. 1996;75(1):19-48.
4. Noda N-A, Kobayashi K, Yagishita M. Variation of mixed modes stress intensity factors of an inclined semi-elliptical surface crack. *Int J Fract*. 1999;100(3):207-225.
5. Noda N-A, Kagita M. Variations of stress intensity factors of a semi-elliptical surface crack subjected to mode I, II, III loading. *Int J Pres Ves pip*. 2004;81(7):635-644.
6. Goto M, Han SZ, Ahn JH, et al. The role of mixed-mode deformation at the crack tip on shear banding and crack propagation of ultrafine-grained copper. *Int J Fatigue*. 2014;66: 220-228.
7. Goto M, Han SZ, Yamamoto T, et al. Formation mechanism of inclined fatigue-cracks in ultrafine-grained Cu processed by equal channel angular pressing. *Int J Fatigue*. 2016;92: 577-587.
8. Goto M, Yamamoto T, Han SZ, et al. Crack growth rate of inclined and deflected surface-cracks in round-bar specimens of copper processed by equal channel angular pressing under cyclic loading. *Eng Fract Mech*. 2017;182: 100-113.
9. Noda N-A, Kihara T, Beppu D. Variation of stress intensity factor of a semi-elliptical surface crack subjected to mixed mode loading. *Int J Fract*. 2004;127(2):167-191.
10. Noda N-A, Sera M, Takase Y. Stress concentration factors for round and flat test specimens with notches. *Int J Fatigue*. 1995; 17(3):163-178.
11. Noda N-A, Takase Y. Stress concentration formula useful for all notch shape in a round bar (comparison between torsion, tension and bending). *Int J Fatigue*. 2006;28(2):151-163.
12. Noda N-A, Takase Y. Theory of Fatigue Notch Strength Useful for Machine Design. Nikkan Kogyo Shinbun 2010. ISBN: 978-4-526-06496-8
13. Irwin GR. Crack-extension force for a part-through crack in a plate. *J Appl Mech*. 1962;29(1):651-654.
14. Bazant ZP, Estenssoro LF. General numerical method for three-dimensional singularities in cracked or notched elastic solids. Proce the 4th Int Conf Fract (Edited by D.M.R. Taplin) 1977;3:371–385., University of Waterloo, Ontario, Canada.
15. Bazant ZP. Three-dimensional harmonic functions near termination or intersection of gradient singularity line: a general numerical method. *Int J Eng Sci*. 1974;12(3):221-243.
16. Benthem JP. On an inversion theorem for conical regions in elasticity theory. *J Elast*. 1979;9(2):159-169.
17. Fujitani Y. Analysis of the stress singular solution in the three-dimensional surface crack problem by Rayleigh-Ritz method. *Bull Hiroshima Univ*. 1980;28:129-137.
18. Barsoum RS. Application of the finite element iterative method to the eigenvalue problem of a crack between dissimilar media. *Int J Numer Methods Eng*. 1988;25(3):541-554.
19. Nakamura T, Parks DM. Three-dimensional elastic stress field near the crack front of a thin elastic plate. *J Appl Mech*. 1988; 55(4):805-813.
20. Nakamura T, Parks DM. Anti-symmetrical 3 D stress field near the crack front of a thin elastic plate. *Int J Solids Struct*. 1989; 25(12):1411-1426.
21. Ghahremani F, Shih CF. Corner singularities of three-dimensional planar interface crack. *J Appl Mech*. 1992;59(1): 61-68.
22. Pook LP. A note on corner point singularities. *Int J Fract*. 1992; 53(1):R3-R8.
23. Pook LP. Some implications of corner point singularities. *Eng Fract Mech*. 1994;48(3):367-378.
24. Dhondt G. On corner point singularities along a quarter circular crack subject to shear loading. *Int J Fract*. 1998;89: L33-L38.
25. Noda N-A, Kihara T, Beppu D. Analysis of variation of stress intensity factor of semi-elliptical surface crack subjected to mixed mode loading. *Trans JSME*. 2001;67-661(661):1542-1547.

26. Noda N-A, Yagishita M, Kihara T. Effect of crack shape, inclination angle, and friction coefficient in crack surface contact problems. *Int J Fract*. 2000;105(4):367-389.
27. Noda N-A, Oda K. Numerical solutions of the singular integral equations in the crack analysis using the body force method. *Int J Fract*. 1992;58(4):285-304.
28. Hadamard J. *Lecture on Cauchy's problem in linear partial differential equations*. Yale University Press.
29. He MY, Hutchinson JW. Surface crack subject to mixed mode loading. *Eng Fract Mech*. 2000;65(1):1-14.
30. Benthem JP. State of stress at the vertex of crack in a half-space. *Int J Solids Struct*. 1977;13(5):479-492.
31. Benthem JP. The quarter-infinite crack in a half space; alternative and additional solutions. *Int J Solids Struct*. 1980;16(2):119-130.
32. Bazant ZP, Estenssoro LF. Surface singularity and crack propagation. *Int J Solids Struct*. 1979;15(5):405-426.
33. Takakuda K. Stress singularity at the crack tip of surface crack. *Trans JSME*. 1984;50:1193-2000. (in Japanese)
34. Murakami Y, Natsume H. Corner point singularity of 3-D crack subjected to mode II loading. *Trans JSME*. 2000;66(652):2211-2217.
35. Otsuka A, Tohgo K, Yoshida M. Fatigue crack growth of a mixed three-dimensional crack (2nd report, fatigue crack growth behavior from a semi-elliptical surface crack under shear loading). *Trans JSME*. 1987;54(505):1735-1744.
36. Murakami Y, Isida M. Analysis of an arbitrarily shaped surface crack and stress field at crack front near surface. *Trans JSME*. 1985;51-464(464):1050-1056.
37. Murakami Y. *Effects of Small Defects and Non-Metallic Inclusions*. Metal Fatigue Elsevier; 2002.
38. Nisitani H, Murakami Y. Stress intensity factors of an elliptical crack or a semi-elliptical crack subject to tension. *Int J Fract*. 1974;10(3):353-368.
39. Isida M, Noguchi H, Yoshida T. Tension and bending of finite thickness plates with a semi-elliptical surface crack. *Int J Fract*. 1984;26(3):157-188.
40. Isida M, Noguchi H. Tension of a plate containing an embedded elliptical crack. *Eng Fract Mech*. 1984;20(3):387-408.
41. Murakami Y, Isida M. Analysis method of stress intensity factor of modes I, II, and III for arbitrarily shaped inclined surface crack. *Trans JSME*. 1984;50-455(455):1359-1366.
42. Isida M, Tsuru H, Noguchi H. New method of analysis of three-dimensional crack problems (1st report, basic theory and applications to infinite body problems). *Trans JSME*. 1993;59-561(561):1270-1278.
43. Noguchi H, Isida M, Tsuru H. New method of analysis of three-dimensional crack problems (2nd report, application to semi-infinite body problems with an arbitrary surface or internal crack under complex loading conditions). *Trans JSME*. 1993;59-561(561):1279-1286.
44. Isida M, Noguchi H. Tension and bending of finite thickness plates with a semi-elliptical surface crack. *Trans JSME*. 1982;48-429(429):607-619.
45. Newman JC Jr, Raju IS. An empirical stress-intensity factor equation for the surface crack. *Eng Fract Mech*. 1979;11:817-829.

How to cite this article: Takase Y, Noda N-A. SIF formula based on exact SIF distribution for semi-elliptical surface cracks subjected to mode I, II, III uniform loading. *Fatigue Fract Eng Mater Struct*. 2024;47(5):1762-1794. doi:10.1111/ffe.14239

APPENDIX A: PREVIOUS STUDIES FOR CORNER POINT SINGULARITY EXPONENT

Table A1 summarizes the previous studies for the corner point singularity exponent p_S under symmetric deformation. As shown in Table A1, although some differences can be seen,, when $\nu \neq 0$, $p_S < 0.5$ and only when $\nu = 0$, $p_S = 0.5$. Table A2 summarizes the previous studies for the corner point singularity exponent p_S under skew-symmetric deformation. As shown in Table A2, although some differences can be seen, when $\nu \neq 0$, $p_A > 0.5$ and only when $\nu = 0$, $p_A = 0.5$. Tables A1 and A2 are useful for surface cracks when the intersection angle at the corner point $\theta_S = 90°$.

TABLE A1 Singularity exponent p_S at corner point to express singular stress under symmetric mode I type deformation.

ν	Ref.[30]	Ref.[31]	Ref.[32]	Ref.[33]
0	0.5	0.49997		0.5002
0.1				0.4904
0.15	0.4836	0.4835	0.484	
0.2				0.4755
0.3	0.4523	0.4519	0.452	0.4523
0.4	0.4132	0.4141	0.413	0.4133
0.5	0.3318	0.3452		0.3316

TABLE A2 Singularity exponent p_A at corner point to express singular stress under skew-symmetric mode II, III type deformation.

ν	Ref.[31]	Ref.[32]
0	0.4999	
0.15	0.5668	0.565
0.3	0.6073	0.598
0.4	0.6286	0.604
0.5	0.6462	

Table A3 shows the maximum SIF $F_{ISE}^{Max} = K_{ISE}^{Max}/(\sigma_0\sqrt{\pi b})$ of a square surface crack under tension and the position by varying Poisson's ratio ν.[36] When $\nu = 0.3$, the maximum SIF F_I^{Max} appears at $y = 4.69 \times 10^{-2} \times a$, which coincides with the position of the maximum SIF of the semicircular crack, that is, $y = sin\,3° = 5.24 \times 10^{-2} \times a$. Murakami-Ishida[36] also investigated that since the region controlled by the corner point singularity is limited in the small range $y = \sim 10^{-3} \times a$. Therefore, the discussion on the corner point singularity is practically meaningless.

Table A4 shows that corner point singularity exponents p_S for symmetric deformation by varying the crack front angle intersecting to free surface θ_S.[33] The results in Table A4 can be used to obtain the crack front angle intersection to free surface θ_S to provide $p_S = 0.5$. The results of Table A4 can be plotted as shown in Figure A1 to obtain θ_S providing $p_S = 0.5$. This paper deals with the semi-elliptical crack in a semi-infinite body under uniform loading as shown in Figure 1A. However, if a semi-elliptical crack is subjected to alternative tensile loading, around the corner point, the crack shape near the free surface will be changed as shown in the figure in Table A4 and Figure A1B because, except at the corner point, the SIF value is quite large, and only at the corner point, the SIF value is zero. Therefore, the formula proposed in this paper in the range $1° \leq \beta \leq 90°$ can be applied to the crack shape in Figure 4 in the range

ν	F_I^{Max}	$(y/a)\|_{x=a}$
0.0	0.955	0
0.1	0.950	1.17×10^{-2}
0.2	0.965	2.34×10^{-2}
0.3	0.992	4.69×10^{-2}
0.4	1.03	4.69×10^{-2}
0.45	1.05	$(4.69 \sim 9.375 \times 10^{-2})$
0.49	1.08	$(4.69 \sim 9.375 \times 10^{-2})$

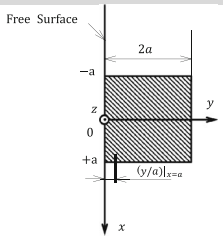

TABLE A3 Maximum stress intensity factor F_I^{Max} of a square surface crack under tension and the position by varying Poisson's ratio ν[36] ($F_{ISE}^{Max} = K_{ISE}^{Max}/(\sigma_0\sqrt{\pi b})$).

TABLE A4 Corner point singularity exponents p_S for symmetric deformation vs crack front angle intersecting to free surface θ_S.[33]

	ν					
θ_S	**0.0**	**0.1**	**0.2**	**0.3**	**0.4**	**0.5**
22.5	0.1325	0.1139	0.0913	0.0646	0.0339	
45	0.3056	0.2852	0.2536	0.2058	0.1313	
67.5	0.4195	0.4054	0.3814	0.3422	0.2727	0.0507
90	0.5002	0.4904	0.4755	0.4523	0.4133	0.3316
112.5	0.5655	0.5597	0.5536	0.546	0.5344	0.5136
135	0.6075	0.6112	0.6174	0.626	0.6364	0.6473
157.5	0.6169	0.6294	0.6482	0.6717	0.6969	0.7211

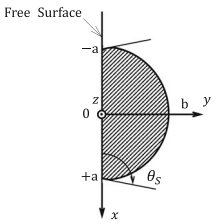

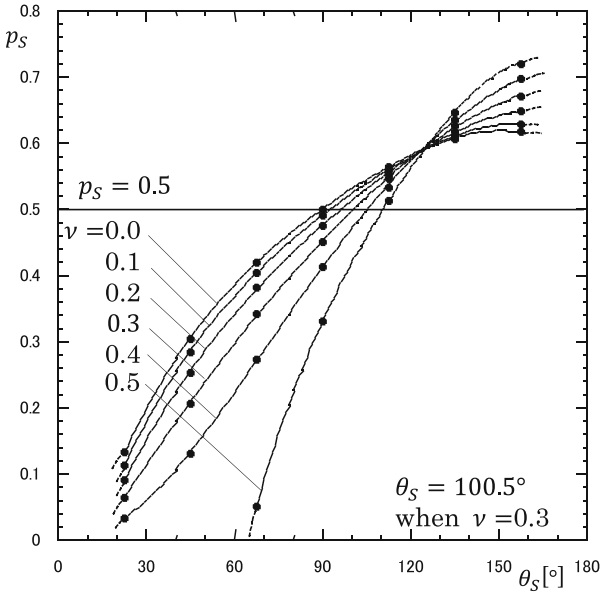

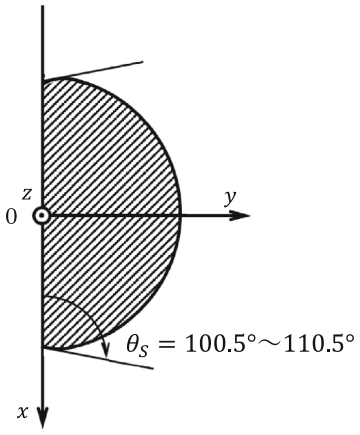

FIGURE A1 Corner point singular exponents p_S for symmetric deformation vs crack front angle intersecting to free surface θ_S.

$0 \le \beta \le 90°$. In other words, since the corner point singularity is meaningless in practice, such semi-elliptical surface crack modeling should be considered such that the crack front intersects the free surface as shown in Figure 4.

APPENDIX B: PREVIOUS STUDIES FOR THE SIF OF A SEMI-ELLIPTICAL SURFACE CRACK

Readers may think that the present results need to be compared to some representative highly accurate and well-accepted literature data obtained by numerical methods. In this section, therefore, the SIF of the proposed formula will be compared with the previous results. For the readers' understanding of the accuracy, the compliance of the boundary condition will be indicated. Several results were previously obtained based on the same hypersingular integral Equation (1) but by using different numerical methods. Those results will be shown for the readers' convenience.

$$\left.\begin{aligned} f^{(j)}(\xi,\eta) &= f_j \cdot w(\xi,\eta), \\ w(\xi,\eta) &= \frac{b\sigma_z^{\infty}}{H\Phi}\sqrt{1-(\xi/a)^2-(\eta/b)^2}, \end{aligned}\right\} \tag{B1a}$$

$$\Phi = \left\{ \begin{array}{c} E(k),\ k = \sqrt{1-(b/a)^2}\ (a \geq b) \\ \dfrac{b}{a}E(k'),\ k' = \sqrt{1-(b/a)^2}\ (a < b) \end{array} \right\}. \quad \text{(B1b)}$$

Figure B1 illustrates the division of the crack region previously used to solve Equation (1) expressing the boundary condition $\sigma_z = 0$. As can be seen in Figure B1, instead of applying polynomial in Equations (3) ~ (5), the unknown function was approximated by the stepped functions or linear functions with Equation (B1). Here, $w(x,y)$ is a fundamental density function of a body force, which expresses the stress field due to an elliptical crack in an infinite body and leads to solutions with high accuracy. Initially, Nisitani-Murakami used a stepped function having a constant value at jth division as shown in Figure B1A to approximate the weight function f_j.[38–40] Murakami-Isida[41] and Isida-Tsuru-Noguchi[42,43] used a linear function $F_j(\xi,\eta)$ expressed in Equation (B2). In those studies,[38–43] the weight functions f_j and $F_j(\xi,\eta)$ were determined from the boundary conditions at collocation points selected in the jth division without considering other points.

$$f^{(j)}(\xi,\eta) = F_j(\xi,\eta)w(\xi,\eta),\ F_j(\xi,\eta) = c_j\xi + d_j\eta + e_j. \quad \text{(B2)}$$

Since no previous study is available for the SIF distribution $F_{ISE}(\beta)$, the SIF at the deepest point $F_{ISE}(90^\circ)$ specified as $\beta = 90^\circ$ in Figure 1A is mainly focused. By using the approximation shown in Figure B1C and Equation (B2), Isida et al. analyzed the semi-elliptical crack and proposed the following formula to estimate the SIF $F_{ISE}(90^\circ)$ at the deepest point.[39,42,43]

$$\begin{aligned} F_{ISE}^{Isida}(90^\circ) &= 1.1526 + 0.1132\nu - 0.0528\nu^2 \\ &\quad + (b/a)\left(-0.7167 - 0.1479\nu + 1.0259\nu^2\right) \\ &\quad + (b/a)^2\left(0.2003 + 0.0347\nu - 0.7182\nu^2\right)\ (0 \leq \nu \leq 0.4, 1.0 \leq a/b \leq 4.0) \end{aligned} \quad \text{(B3)}$$

As indicated in Section 2, in the present analysis, polynomials have been used to approximate the unknown functions as a continuous function. Figure B2A~C illustrate the compliance of the boundary conditions along the prospective crack surface with varying n in Equation (5). The boundary condition, that is, $\sigma_z = 0$, becomes highly satisfied with increasing n. When Poisson's ratio $\nu = 0.3$ and $n = 18$, the error is less than 3×10^{-3} throughout the crack region. The boundary condition is more highly satisfied when $\nu = 0$ within the error 1×10^{-3}. From those figures examining the boundary condition and the convergence shown in Tables 1 and 2, it can be conjectured that the solutions indicated in Sections 3 and 4 have more than three-digit accuracy and are more accurate and reliable than any other results. Similarly, when the semi-elliptical surface crack is subjected to remote shear in Figure 1C, the compliance of the boundary conditions, that is, $\tau_{yz} = 0$, $\tau_{zx} = 0$, are examined in reference[9]. For example, Figure B2D illustrates the boundary condition $\tau_{yz} = 0$ when $n = 15, \nu = 0.3, a/b = 1$.

Table B1 shows the present results discussed in Section 3 under remote tension and several previous results. As indicated above, the most reliable mode I SIF, F_{ISE}^{N-M} of Noda-Miyoshi[3,26] and the value of formula $F_{ISE}^{Eq(8)}$ in Equation (8) are compared with $F_{ISE}^{Isida}(90^\circ)$ in Equation (B3),[39] F_{ISE}^{I-N} of Isida-Noguchi,[44] and F_{ISE}^{R-N} of Raju-Newman.[45] As shown in Table B1, the accuracy of those previous results can be confirmed from the ratio

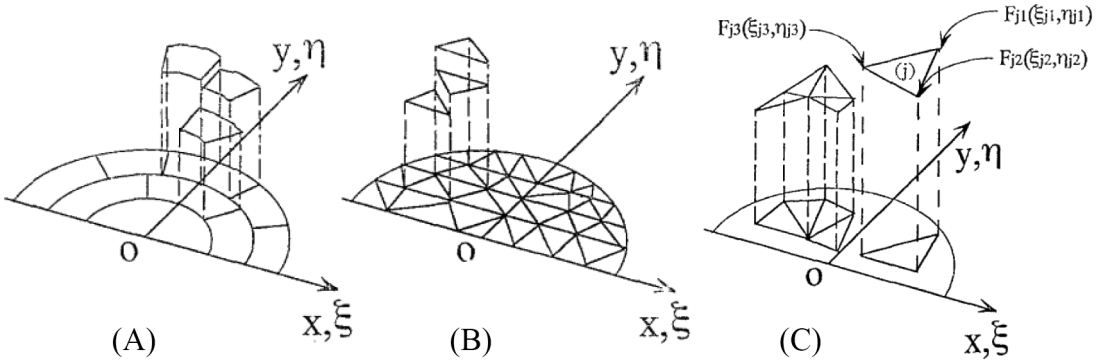

FIGURE B1 Approximation of weighting function using the step function at each element. (A) Nisitani-Murakami[38] and Isida-Noguchi-Yoshida,[39,40] (B) Murakami-Isida,[41] and (C) Isida-Tsuru-Noguchi.[42,43]

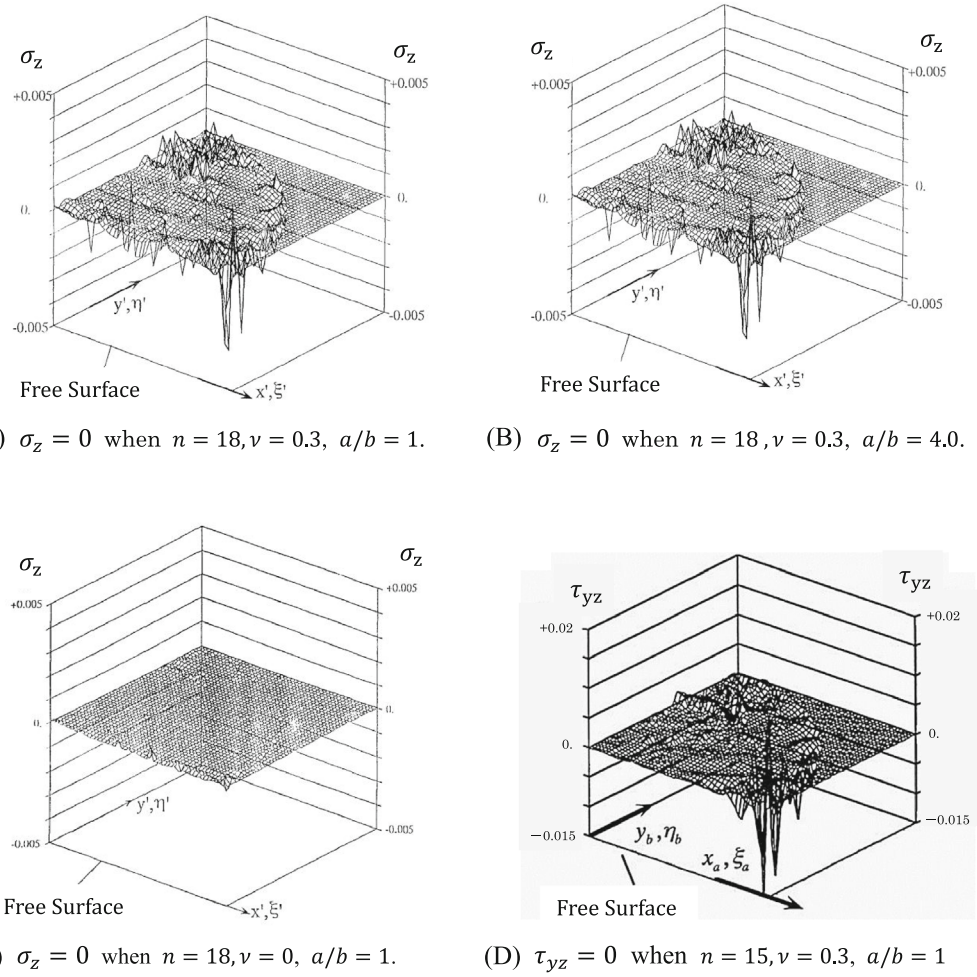

(A) $\sigma_z = 0$ when $n = 18, \nu = 0.3,\ a/b = 1.$ (B) $\sigma_z = 0$ when $n = 18, \nu = 0.3,\ a/b = 4.0.$

(C) $\sigma_z = 0$ when $n = 18, \nu = 0,\ a/b = 1.$ (D) $\tau_{yz} = 0$ when $n = 15, \nu = 0.3,\ a/b = 1$

FIGURE B2 Compliance of boundary condition $\sigma_z = 0$ or $\tau_{yz} = 0$. (A) $\sigma_z = 0$ when $n = 18, \nu = 0.3, a/b = 1$. (B) $\sigma_z = 0$ when $n = 18, \nu = 0.3, a/b = 4.0$. (C) $\sigma_z = 0$ when $n = 18, \nu = 0, a/b = 1$. (D) $\tau_{yz} = 0$ when $n = 15, \nu = 0.3, a/b = 1$.

$F_{ISE}^{N-M}/F_{ISE}^{N-M}$, $F_{ISE}^{Eq(8)}/F_{ISE}^{N-M}$, $F_{ISE}^{Isida}/F_{ISE}^{N-M}$, $F_{ISE}^{I-N}/F_{ISE}^{N-M}$, and $F_{ISE}^{R-N}/F_{ISE}^{N-M}$. Equation (B3) provides the SIF at the deepest point within 0.5% error since $F_{ISE}^{Ishida}(90°)$ agrees well with F_{ISE}^{N-M}. Since Isida-Noguchi used the linear function approximation in Equation (B2), it is difficult to obtain the SIF around the corner point. Therefore, only when $a/b = 1.0$, Isida-Noguchi provided the SIF around the corner point at $\beta \approx \sim 3°$. The result coincides with the present results within 0.5% error. The result of Raju-Newman F_{ISE}^{R-N}[45] when $a/b = 1.0/0.6 = 1.\dot{6}$ coincides with the present result within 1.3% error.

Tables B2 and B3 show the present results when the semi-elliptical crack is subjected to remote shear as discussed in Section 4. The most reliable SIFs F_{IISE}^{N-K-B}, F_{IIISE}^{N-K-B} of Noda-Kihara-Beppu[9] and the value of formula $F_{IISE}^{Eq(14)}$ in Equation (14) and $F_{IIISE}^{Eq(16)}$ in Equation (16) are compared with the previous results F_{IISE}^{H-H}, F_{IIISE}^{H-H} obtained by He-Hutchinson.[29] As shown in Tables B2 and B3, the accuracy of F_{IISE}^{H-H}, F_{IIISE}^{H-H} can be confirmed from the ratio $F_{IISE}^{H-H}/F_{IISE}^{N-K-B}$ and $F_{IIISE}^{H-H}/F_{IIISE}^{N-K-B}$. Note that the values of F_{IISE}^{H-H} in Table B2 and the values of F_{IIISE}^{H-H} in Table B3 are taken from the charts in Ref.[29] From Tables B2, it is seen that the results of F_{IISE}^{H-H} agree with the present results within 3% error. Also, it is seen that the F_{IIISE}^{H-H} results agree with the present results within about 3% in most cases; however, only some cases in the range $\beta \leq 8°$, F_{IIISE}^{H-H} has less than or equal to about 8% error. He-Hutchinson[29] also considered the exact solution of the elliptical crack in an infinite body. However, for mode III SIF in the range $\beta \leq 8°$, as shown in Tables 5 and 6, the semi-elliptical crack solution F_{IIISE} is totally different from the exact solution of the elliptical crack F_{IIIE}. This may be the reason why about 8% appears in $F_{IIISE}^{H-H}(\beta)$.

TABLE B1 Most accurate F_{ISE}^{N-M} of Noda-Miyoshi[3] and $F_{ISE}^{Eq(8)}$ of Equation (8) in comparison with F_{ISE}^{Isida} of Equation (B3),[39] F_{ISE}^{I-N} of Isida-Noguchi F_{ISE}^{I-N},[44] and F_{ISE}^{R-N} of Raju-Newman[45] for $a/b = 1.0 \sim 4.0, \nu = 0.3$ [$A/A = F_{ISE}^{N-M}/F_{ISE}^{N-M}$, $B/A = F_{ISE}^{Eq(8)}/F_{ISE}^{N-M}$, $C/B = F_{ISE}^{Isida}/F_{ISE}^{Eq(8)}$, $D/A = F_{ISE}^{I-N}/F_{ISE}^{N-M}$, $E/A = F_{ISE}^{R-N}/F_{ISE}^{N-M}$].

	F_{ISE}										F_{ISE}					
	F_{ISE} ($\beta = 90°$)										F_{ISE} ($\beta \approx \sim 3°$)					
	A	B	C	D	E	Ratio to F_{ISE}^{N-M}					A	B	D	Ratio to F_{ISE}^{N-M}		
a/b	F_{ISE}^{N-M}[3]	$F_{ISE}^{Eq(8)}$	F_{ISE}^{Isida}[39]	F_{ISE}^{I-N}[44]	F_{ISE}^{R-N}[45]	$\frac{A}{A}$	$\frac{B}{A}$	$\frac{C}{B}$	$\frac{D}{A}$	$\frac{E}{A}$	F_{ISE}^{N-M}[3]	$F_{ISE}^{Eq(8)}$	F_{ISE}^{I-N}[44]	$\frac{A}{A}$	$\frac{B}{A}$	$\frac{D}{A}$
1.0	0.6585	0.6585	0.6591	0.660	-	1.0	1.0	1.001	1.002	-	0.748	0.7476	0.7448	1.0	0.999	0.996
1.18	-	0.7178	0.7200	-	-	1.0	~ 1	1.003	-	-	-	0.7472	-	1.0	~ 1	-
1.19	-	0.7208	0.7230	-	-	1.0	~ 1	1.003	-	-	-	0.7470	-	1.0	~ 1	-
1.20	-	0.7237	0.7260	-	-	1.0	~ 1	1.003	-	-	-	0.7468	-	1.0	~ 1	-
1.21	-	0.7266	0.7289	-	-	1.0	~ 1	1.003	-	-	-	0.7465	-	1.0	~ 1	-
1.22	-	0.7295	0.7318	-	-	1.0	~ 1	1.003	-	-	-	0.7463	-	1.0	~ 1	-
1.23	-	0.7323	0.7347	-	-	1.0	~ 1	1.003	-	-	-	0.7460	-	1.0	~ 1	-
1.24	-	0.7351	0.7375	-	-	1.0	~ 1	1.003	-	-	-	0.7458	-	1.0	~ 1	-
1.25	-	0.7379	0.7403	-	-	1.0	~ 1	1.003	-	-	-	0.7455	-	1.0	~ 1	-
1.26	-	0.7406	0.7431	-	-	1.0	~ 1	1.003	-	-	-	0.7452	-	1.0	~ 1	-
1.27	-	0.7433	0.7458	-	-	1.0	~ 1	1.003	-	-	-	0.7449	-	1.0	~ 1	-
1.28	-	0.7460	0.7485	-	-	1.0	~ 1	1.003	-	-	-	0.7446	-	1.0	~ 1	-
1.29	-	0.7487	0.7512	-	-	1.0	~ 1	1.003	-	-	-	0.7442	-	1.0	~ 1	-
1.30	-	0.7513	0.7538	-	-	1.0	~ 1	1.003	-	-	-	0.7439	-	1.0	~ 1	-
$1.\dot{3}$	0.7598	0.7598	0.7624	-	-	1.0	1.0	1.003	-	-	0.743	0.7426	-	1.0	0.999	-
$1.6\dot{6}$	-	0.8310	0.8331	0.831	0.842	1.0	~ 1	1.003	-	~ 1.013	-	0.7267	-	1.0	~ 1	-
2.0	0.8835	0.8830	0.8840	0.883	-	1.0	1.0	1.001	0.999	-	0.710	0.7096	-	1.0	0.999	-
4.0	1.023435	1.0231	1.0238	1.022	-	1.0	1.0	1.001	0.999	-	0.601	0.6009	-	1.0	1.000	-

TABLE B2 Most accurate $F_{IISE}^{N-K-B}(\beta)$ of Noda-Kihara-Beppu[9] and $F_{IISE}^{Eq(14)}(\beta)$ in Equation (14) in comparison with $F_{IISE}^{H-H}(\beta)$ of He-Hutchinson[29] for $a/b = 1.0 \sim 2.0, \nu = 0.3$ [$A/A = F_{IISE}^{N-K-B}/F_{IISE}^{N-K-B}$, $B/A = F_{IISE}^{Eq(14)}/F_{IISE}^{N-K-B}$, $C/A = F_{IISE}^{H-H}/F_{IISE}^{N-K-B}$].

	a/b																	
	1.0						1.5						2.0					
	A	B	C	Ratio to F_{IISE}^{N-K-B}			A	B	C	Ratio to F_{IISE}^{N-K-B}			A	B	C	Ratio to F_{IISE}^{N-K-B}		
β (°)	F_{IISE}^{N-K-B}[9]	$F_{IISE}^{Eq(14)}$	F_{IISE}^{H-H}[29]	$\frac{A}{A}$	$\frac{B}{A}$	$\frac{C}{A}$	F_{IISE}^{N-K-B}[9]	$F_{IISE}^{Eq(14)}$	F_{IISE}^{H-H}[29]	$\frac{A}{A}$	$\frac{B}{A}$	$\frac{C}{A}$	F_{IISE}^{N-K-B}[9]	$F_{IISE}^{Eq(14)}$	F_{IISE}^{H-H}[29]	$\frac{A}{A}$	$\frac{B}{A}$	$\frac{C}{A}$
1	0.765	0.7641	-	1.000	0.999	-	0.779	0.7785	-	1.000	0.999	-	0.779	0.7789	-	1.000	1.000	-
2	0.744	0.7447	-	1.000	1.001	-	0.740	0.7418	-	1.000	1.002	-	0.732	0.7333	-	1.000	1.002	-
3	0.733	0.7327	-	1.000	1.000	-	0.723	0.7224	-	1.000	0.999	-	0.707	0.7071	-	1.000	1.000	-
4	0.726	0.7255	-	1.000	0.999	-	0.716	0.7147	-	1.000	0.998	-	0.696	0.6943	-	1.000	0.998	-
5	0.720	0.7155	0.692	1.000	0.994	0.961	0.713	0.7122	0.708	1.000	0.999	0.993	0.689	0.6893	0.715	1.000	1.000	1.038
6	0.715	0.7124	0.687	1.000	0.996	0.961	0.709	0.7084	0.704	1.000	0.999	0.993	0.684	0.6840	0.706	1.000	1.000	1.032
7	0.709	0.7093	0.684	1.000	1.000	0.965	0.704	0.7044	0.701	1.000	1.001	0.996	0.679	0.6783	0.690	1.000	0.999	1.016
8	0.704	0.7062	0.683	1.000	1.003	0.970	0.700	0.7002	0.699	1.000	1.000	0.999	0.673	0.6722	0.684	1.000	0.999	1.016
9	0.700	0.7029	0.682	1.000	1.004	0.974	0.695	0.6958	0.690	1.000	1.001	0.993	0.666	0.6659	0.679	1.000	1.000	1.020
10	0.696	0.6997	0.681	1.000	1.005	0.978	0.691	0.6911	0.686	1.000	1.000	0.993	0.659	0.6593	0.671	1.000	1.000	1.018
20	0.6635	0.6622	0.656	1.000	0.998	0.989	0.6342	0.6342	0.625	1.000	1.000	0.985	0.5817	0.5822	0.582	1.000	1.001	1.001
30	0.6139	0.6117	0.608	1.000	0.996	0.990	0.5620	0.5614	0.559	1.000	0.999	0.995	0.4964	0.4959	0.494	1.000	0.999	0.995
40	0.5453	0.5443	0.540	1.000	0.998	0.990	0.4779	0.4777	0.471	1.000	1.000	0.986	0.4094	0.4090	0.408	1.000	0.999	0.997
50	0.4591	0.4589	0.456	1.000	1.000	0.993	0.3871	0.3869	0.384	1.000	0.999	0.992	0.3241	0.3240	0.319	1.000	1.000	0.984
60	0.3580	0.3575	0.352	1.000	0.999	0.983	0.2925	0.2921	0.289	1.000	0.999	0.988	0.2410	0.2410	0.238	1.000	1.000	0.988
70	0.2453	0.2442	0.242	1.000	0.996	0.987	0.1957	0.1953	0.194	1.000	0.998	0.991	0.1597	0.1597	0.156	1.000	1.000	0.977
80	0.1247	0.1238	0.123	1.000	0.993	0.986	0.0980	0.0979	0.097	1.000	0.999	0.990	0.0798	0.0796	0.077	1.000	0.997	0.965
90	0	0	0	-	-	-	0	0	0	-	-	-	0	0	0	-	-	-

TABLE B3 Most accurate $F_{IIISE}^{N-K-B}(\beta)$ of Noda-Kihara-Beppu[9] and $F_{IIISE}^{Eq(16)}$ in Equation (16) in comparison with $F_{IIISE}^{H-H}(\beta)$ of He-Hutchinson[29] for $a/b = 1.0 \sim 2.0, \nu = 0.3$ $[A/A = F_{IIISE}^{N-K-B}/F_{IIISE}^{N-K-B},\ B/A = F_{IIISE}^{Eq(16)}/F_{IIISE}^{N-K-B},\ C/A = F_{IIISE}^{H-H}/F_{IIISE}^{N-K-B}]$.

	a/b																	
	1.0						1.5						2.0					
	A	B	C	Ratio to F_{IIISE}^{N-K-B}			A	B	C	Ratio to F_{IIISE}^{N-K-B}			A	B	C	Ratio to F_{IIISE}^{N-K-B}		
β (°)	F_{IIISE}^{N-K-B}[9]	$F_{IIISE}^{Eq(16)}$	F_{IIISE}^{H-H}[29]	$\frac{A}{A}$	$\frac{B}{A}$	$\frac{C}{A}$	F_{IIISE}^{N-K-B}[9]	$F_{IIISE}^{Eq(16)}$	F_{IIISE}^{H-H}[29]	$\frac{A}{A}$	$\frac{B}{A}$	$\frac{C}{A}$	F_{IIISE}^{N-K-B}[9]	$F_{IIISE}^{Eq(16)}$	F_{IIISE}^{H-H}[29]	$\frac{A}{A}$	$\frac{B}{A}$	$\frac{C}{A}$
1	0.284	0.2832	-	1.000	0.997	-	0.307	0.3068	-	1.000	0.999	-	0.311	0.3113	-	1.000	1.001	-
2	0.238	0.2394	-	1.000	1.006	-	0.257	0.2572	-	1.000	1.001	-	0.267	0.2662	-	1.000	0.997	-
3	0.216	0.2166	-	1.000	1.003	-	0.232	0.2321	-	1.000	1.000	-	0.242	0.2423	-	1.000	1.001	-
4	0.208	0.2070	-	1.000	0.995	-	0.223	0.2230	-	1.000	1.000	-	0.233	0.2333	-	1.000	1.001	-
5	0.206	0.2047	0.211	1.000	0.994	1.024	0.224	0.2233	0.236	1.000	0.997	1.054	0.234	0.2341	0.253	1.000	1.000	1.081
6	0.206	0.2054	0.210	1.000	0.997	1.019	0.229	0.2285	0.233	1.000	0.998	1.017	0.241	0.2408	0.260	1.000	0.999	1.079
7	0.206	0.2068	0.210	1.000	1.004	1.019	0.235	0.2353	0.237	1.000	1.001	1.009	0.251	0.2506	0.267	1.000	0.998	1.064
8	0.206	0.2075	0.210	1.000	1.007	1.019	0.242	0.2421	0.243	1.000	1.000	1.004	0.262	0.2618	0.273	1.000	0.999	1.042
9	0.207	0.2071	0.211	1.000	1.000	1.019	0.248	0.2480	0.249	1.000	1.000	1.004	0.273	0.2730	0.281	1.000	1.000	1.029
10	0.208	0.2062	0.211	1.000	0.991	1.014	0.254	0.2532	0.259	1.000	0.997	1.020	0.284	0.2840	0.293	1.000	1.000	1.032
20	0.2509	0.2536	0.255	1.000	1.011	1.016	0.3381	0.3401	0.340	1.000	1.006	1.006	0.3974	0.3991	0.393	1.000	1.004	0.989
30	0.3108	0.3088	0.312	1.000	0.994	1.004	0.4255	0.4239	0.420	1.000	0.996	0.987	0.5003	0.4989	0.491	1.000	0.997	0.981
40	0.3716	0.3716	0.371	1.000	1.000	0.998	0.5022	0.5020	0.499	1.000	1.000	0.994	0.5836	0.5835	0.581	1.000	1.000	0.996
50	0.4273	0.4299	0.426	1.000	1.006	0.997	0.5648	0.5666	0.560	1.000	1.003	0.992	0.6484	0.6499	0.642	1.000	1.002	0.990
60	0.4739	0.4742	0.471	1.000	1.001	0.994	0.6127	0.6127	0.607	1.000	1.000	0.991	0.6969	0.6969	0.691	1.000	1.000	0.992
70	0.5088	0.5073	0.506	1.000	0.997	0.994	0.6464	0.6448	0.645	1.000	0.998	0.998	0.7305	0.7294	0.730	1.000	0.998	0.999
80	0.5305	0.5334	0.532	1.000	1.005	1.003	0.6663	0.6677	0.666	1.000	1.002	1.000	0.7505	0.7518	0.753	1.000	1.002	1.003
90	0.5370	0.5365	0.537	1.000	0.999	1.000	0.6730	0.6716	0.672	1.000	0.998	0.999	0.7566	0.7556	0.760	1.000	0.999	1.004